ISSN 0924-090X, Volume 60, Number 4

Vol. 60, No. 4, June 2010 ISSN 0924-090X

Nonlinear Dynamics

An International Journal of
Nonlinear Dynamics and Chaos in Engineering Systems

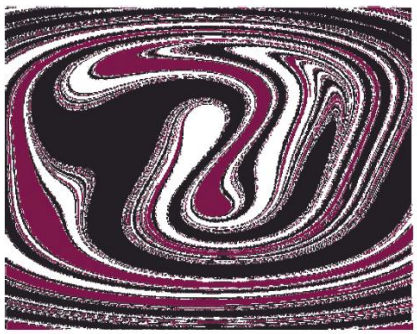

Springer

Nonlinear Dyn (2010) 60: 575–595
DOI 10.1007/s11071-009-9616-7

ORIGINAL PAPER

Analysis of a frictional oblique impact observed in skew bridges

Elias G. Dimitrakopoulos

Received: 5 August 2009 / Accepted: 21 October 2009 / Published online: 27 November 2009

Abstract The oblique contact/impact of skew bridges triggers a unique rotational mechanism which earthquake reconnaissance reports correlate with deck unseating of such bridges. Building on the work of other researchers, the present study adopts a fully nonsmooth rigid body approach and set-valued force laws, in order to analyze in depth this oblique multi-impact phenomenon. A linear complementarity formulation is proposed which yields a great variety of (multi-) impact states, depending on the initial (pre-impact) conditions, such as "slip" or "stick" at one corner (single-impact) or two corners (double-impact) of the body. The pertinent existential conditions of those impact states reveal a complex dynamic behavior. With respect to the rotational mechanism associated with double-impact, the physically feasible impact states as well as, counter-intuitive exceptions are recognized. The study proves that double oblique impact, both frictionless and frictional, may or may not produce rotation of the body and proposes criteria that distinguish each case. Most importantly, it is shown that the tendency of skew bridges to rotate (and hence unseat) after deck-abutment collisions is not a factor of the skew angle alone, but rather of the overall geometry in-plan, plus the impact parameters (coefficient of restitution and coefficient of friction). The study also provides a theoretical justification of the observed tendency of skew bridges to jam at the obtuse corner and rotate in such a way that the skew angle increases. Finally, counter-intuitive trends hidden in the response are unveiled which indicate that, due to friction, a skew bridge may also rotate so that the skew angle decreases.

Keywords Oblique impact · Friction · Unilateral contact · Complementarity · Skew bridges · Concrete bridges

E.G. Dimitrakopoulos (✉)
Department of Civil Engineering, Aristotle University of Thessaloniki, Thessaloniki 54124, Greece
e-mail: ilias.dimitrakopoulos@gmail.com

1 Introduction

This paper focuses on the impact response of skew bridges with deck-abutment expansion joints, while it belongs to a broader study [1–3] on the problem of the earthquake-induced pounding in (straight and skew) bridges.

Skew bridges exhibit a unique seismic response that is triggered by oblique impact. Earthquake reconnaissance reports [4] indicate that skew bridges often rotate in the horizontal plane, thus tending to drop off the supports at the acute corners [5] (Fig. 1). This behavior results in a coupling of longitudinal and transversal response, binding in one of the obtuse corners and subsequently rotation in the direction of increasing the skew angle [5] (Fig. 2).

Despite the recorded evidence from previous earthquakes, which underlines the importance of this mech-

Fig. 1 Damage of a skew bridge after the Tehuacan 1999 Mexico earthquake [6]

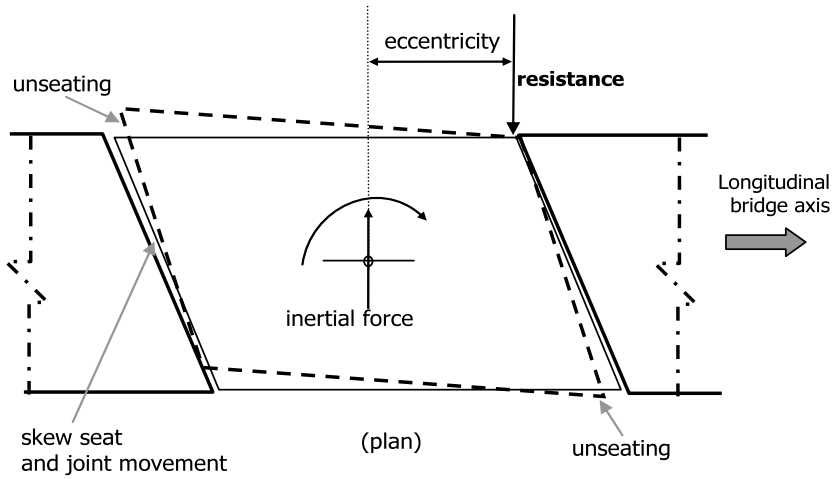

Fig. 2 Rotation mechanism of skew bridges—unseating, adopted from [5]

anism, as well as the empirical vulnerability methodologies that acknowledge skew as a primary vulnerability factor in bridges [7], there are only a few attempts to comprehend this mechanism. One of the first was made by Maragakis et al. [8], motivated after the aforementioned type of damage during the 1971 San Fernando earthquake [4]. Maragakis et al. [8] focused on the rigid body motions of a skew bridge, using a rigid stick model of the bridge deck and spring elements to model piers. Pounding with the abutments was simulated with an elastic spring activated after the closure of the gap. More recently, Maleki [9] studied single-span straight and skew bridges using a SDOF model, in an attempt to estimate the forces developed during collision.

In the vast majority of pertinent studies, including the aforementioned ones, impact is considered as centric and is simulated with a contact-element ("compliance") method. However, contact in skew bridges is oblique and multi-point (multi-impact), and disregarding this fact should be attributed to inherent difficulties in properly modeling it. As a consequence, there is a lack of a thorough theoretical investigation, and hence understanding, regarding this peculiarity of skew bridges.

An alternative way to deal with such an impact and investigate in depth the associated rotational mechanism is within the context of non-smooth dynamics. Key feature of this approach, originating from the pioneering studies of Moreau [10] and Panagiotopoulos [11, 12], is the inequality form of the impact laws which often is transformed to linear complementarity. Notions of convex analysis, as well as set-valued (force) laws, have been embedded naturally within this

context [13]. In recent years an ever increasing number of structural problems is tackled with the notions of non-smooth dynamics; for instance the seismic behavior of pounding structures where unilateral contact configurations (impacts, continuous contacts, and detachments) are mathematically treated as inequality problems by Dimitrakopoulos et al. [3].

Within the framework of an event-based methodology [13–15] the seismic response of a bridge can be decomposed into discontinuous events (e.g. impacts) and continuous impact-free motion. Adopting this standpoint, the main gap in the existing knowledge regarding the seismic response of skew bridges is the phenomenon of the aforementioned oblique multi-impact (Fig. 2). The key objective of this paper is to fill this gap and at the same time to illustrate the effectiveness of non-smooth dynamics in a case with practical significance and multidisciplinary interest. The motivation for this study originates from: (i) the need to elucidate the oblique impact response of skew bridges with deck-abutment joints, (ii) the importance of this rotational mechanism manifested by empirical evidence and recognized by empirical vulnerability methodologies for bridges, and (iii) the large number of existing bridges of this type worldwide.

2 Proposed methodology

In [16] Payr and Glocker re-examined a benchmark problem of impact dynamics illustrating the effectiveness of their non-smooth set-valued approach when compared with more conventional methodologies. The present study builds on the work of Payr and Glocker [16] extending their approach from single to a multiple (double) frictional collision case, which encapsulates a lot of the 'physics' of deck-abutment impact in skew bridges. The bridge deck (in-between two successive separation joints) is considered as a rigid body moving in plane and the interaction between deck and abutment is modeled as a unilateral contact.

Herein the most fundamental impact laws are adopted in a set-valued form following [16]. Impact is assumed to behave according to Newton's law in the normal direction and according to Coulomb's friction law in the transversal direction. Hence, only two impact parameters are needed to describe frictional impact, the normal coefficient of restitution ε_N and the coefficient of friction μ. It is reminded that Newton's coefficient of restitution is taken as the ratio of

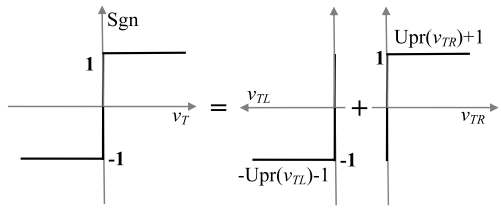

Fig. 3 Set-valued friction force law [16]

the (relative) contact velocities after, $\mathbf{u}^+$, and before, $\mathbf{u}^-$, impact: $u^+ = -\varepsilon_N u^-$ and it varies between zero and one, $\varepsilon_N \in [0, 1]$. In the transversal direction a zero coefficient of restitution is assumed $\varepsilon_T = 0$.

Two set-valued maps, the unilateral primitive (Fig. 3, right) and the Sgn(x) function (Fig. 3, left) are adopted in the normal, Λ_{Ni}, and the transversal, Λ_{Ti}, direction of impact i, respectively:

$$-\Lambda_{Ni} \in \mathrm{Upr}(v_{Ni}) \qquad -\Lambda_{Ti} \in \mu_i \Lambda_{Ni}\, \mathrm{Sgn}(v_{Ti}) \tag{1}$$

Velocities v_N, v_{TR} and v_{TL} are defined later on with (8), (9), and (10).

The $\mathrm{Sgn}(x)$ function differs from the standard sgn function, in the point $x = 0$ where the former yields a set of values: $\mathrm{Sgn}(x = 0) = [-1, 1]$, instead of a single value $\mathrm{sgn}(x = 0) = 0$. In [16], it is shown that the Sgn function can be decomposed into two unilateral primitives (Fig. 3), which is ideal when the problem of impact is formulated as an inequality problem. With the help of Fig. 3 the following decomposition can be achieved:

$$\begin{cases} -\Lambda_{TRi} \in \mathrm{Upr}(v_{TRi}) & \Lambda_{TRi} = \mu\Lambda_{Ni} + \Lambda_{Ti} \\ -\Lambda_{TLi} \in \mathrm{Upr}(v_{TLi}) & \Lambda_{TLi} = \mu\Lambda_{Ni} - \Lambda_{Ti} \\ v_{Ti} = v_{TRi} - v_{TLi} \end{cases} \tag{2}$$

or in vector form:

$$\boldsymbol{\Lambda}_{TL} = \bar{\bar{\mu}}\boldsymbol{\Lambda}_N - \boldsymbol{\Lambda}_T = 2\bar{\bar{\mu}}\boldsymbol{\Lambda}_N - \boldsymbol{\Lambda}_{TR} \tag{3}$$

where $\bar{\bar{\mu}} = \mathrm{diag}\{\mu_i\}$, $\boldsymbol{\Lambda}_N = \{\Lambda_{Ni}\}$, $\boldsymbol{\Lambda}_T = \{\Lambda_{Ti}\}$, $\boldsymbol{\Lambda}_{TL} = \{\Lambda_{TLi}\}$, $\boldsymbol{\Lambda}_{TR} = \{\Lambda_{TRi}\}$.

The problem of frictional multi-impact is formulated herein as a linear complementarity problem (LCP). In the classical form, an LCP is a system of linear equations: $\mathbf{y} = \mathbf{A}\mathbf{x} + \mathbf{b}$, with matrices $\mathbf{A}$ and $\mathbf{b}$ known, and $\mathbf{y}$ and $\mathbf{x}$ the unknown vectors under determination, for which the following additional complementarity conditions hold: $\mathbf{y} \geq 0, \mathbf{x} \geq 0, \mathbf{y}^T\mathbf{x} = 0$. More details on the LCP as well as an overview of the

available algorithms for treating numerically an LCP can be found in [17].

Newton–Euler equations in integrated form, taking into account transversal forces (friction), read as follows:

$$\mathbf{M}(\mathbf{u}^+ - \mathbf{u}^-) = \mathbf{W}_N \boldsymbol{\Lambda}_N + \mathbf{W}_T \boldsymbol{\Lambda}_T \tag{4}$$

where $\boldsymbol{\Lambda}_N$ and $\boldsymbol{\Lambda}_T$ are the impulse vectors in the normal and the transversal direction of impact, respectively, $\mathbf{M}$ is the mass matrix and $\mathbf{W}$ are the direction vectors of the constraints (impact) in the normal (sub-index N) $\mathbf{W}_N = \{\mathbf{w}_{Ni}\}$ and the transversal (sub-index T) $\mathbf{W}_T = \{\mathbf{w}_{Ti}\}$ direction; sub-indexes N, T are used throughout this paper in the same sense. By pre-multiplying with $\mathbf{W}_N^T\mathbf{M}^{-1}$ and $\mathbf{W}_T^T\mathbf{M}^{-1}$, (4) is converted to relative velocities in the normal, $\gamma_{Ni} = \mathbf{w}_{Ni}^T\mathbf{u}$, and the transversal, $\gamma_{Ti} = \mathbf{w}_{Ti}^T\mathbf{u}$, direction of impact, respectively:

$$\begin{aligned} \boldsymbol{\gamma}_N^+ - \boldsymbol{\gamma}_N^- &= \mathbf{W}_N^T\mathbf{M}^{-1}\mathbf{W}_N\boldsymbol{\Lambda}_N + \mathbf{W}_N^T\mathbf{M}^{-1}\mathbf{W}_T\boldsymbol{\Lambda}_T \\ \boldsymbol{\gamma}_T^+ - \boldsymbol{\gamma}_T^- &= \mathbf{W}_T^T\mathbf{M}^{-1}\mathbf{W}_N\boldsymbol{\Lambda}_N + \mathbf{W}_T^T\mathbf{M}^{-1}\mathbf{W}_T\boldsymbol{\Lambda}_T \end{aligned} \tag{5}$$

In (5) and throughout this paper superscript "+" refers to the post-impact state, while super-script "−" to the pre-impact state and $\boldsymbol{\gamma} = \{\gamma_i\}$. Using the notation of Pfeiffer [18]:

$$\begin{aligned} \mathbf{G}_{NN} &= \mathbf{W}_N^T\mathbf{M}^{-1}\mathbf{W}_N \qquad \mathbf{G}_{NT} = \mathbf{W}_N^T\mathbf{M}^{-1}\mathbf{W}_T \\ \mathbf{G}_{TN} &= \mathbf{W}_T^T\mathbf{M}^{-1}\mathbf{W}_N \qquad \mathbf{G}_{TT} = \mathbf{W}_T^T\mathbf{M}^{-1}\mathbf{W}_T \end{aligned} \tag{6}$$

Equations (5) are rewritten as

$$\begin{aligned} \boldsymbol{\gamma}_N^+ - \boldsymbol{\gamma}_N^- &= \mathbf{G}_{NN}\boldsymbol{\Lambda}_N + \mathbf{G}_{NT}\boldsymbol{\Lambda}_T \\ \boldsymbol{\gamma}_T^+ - \boldsymbol{\gamma}_T^- &= \mathbf{G}_{TN}\boldsymbol{\Lambda}_N + \mathbf{G}_{TT}\boldsymbol{\Lambda}_T \end{aligned} \tag{7}$$

The following velocity jumps are defined:

$$\begin{aligned} \mathbf{v}_N &\doteq \boldsymbol{\gamma}_N^+ + \bar{\bar{\varepsilon}}_N\boldsymbol{\gamma}_N^- \\ \mathbf{v}_T &\doteq \boldsymbol{\gamma}_T^+ = \mathbf{v}_{TR} - \mathbf{v}_{TL} \end{aligned} \tag{8}$$

In the normal direction of the impact, the following relation holds:

$$\left.\begin{aligned} &\mathbf{v}_N \doteq \boldsymbol{\gamma}_N^+ + \bar{\bar{\varepsilon}}_N\boldsymbol{\gamma}_N^- \\ &\boldsymbol{\gamma}_N^+ = \boldsymbol{\gamma}_N^- + \mathbf{G}_{NN}\boldsymbol{\Lambda}_N + \mathbf{G}_{NT}\boldsymbol{\Lambda}_T \\ &\boldsymbol{\Lambda}_T = \boldsymbol{\Lambda}_{TR} - \bar{\bar{\mu}}\boldsymbol{\Lambda}_N \end{aligned}\right\} \Rightarrow$$

$$\begin{aligned} \mathbf{v}_N = {} & (\mathbf{G}_{NN} - \mathbf{G}_{NT}\bar{\bar{\mu}})\boldsymbol{\Lambda}_N + \mathbf{G}_{NT}\boldsymbol{\Lambda}_{TR} \\ & + (\bar{\bar{\varepsilon}}_N + \mathbf{E})\boldsymbol{\gamma}_T^- \end{aligned} \tag{9}$$

Similarly in the transversal direction:

$$\left.\begin{aligned} &\mathbf{v}_T = \mathbf{v}_{TR} - \mathbf{v}_{TL} \\ &\boldsymbol{\gamma}_T^+ = \boldsymbol{\gamma}_T^- + \mathbf{G}_{TN}\boldsymbol{\Lambda}_N + \mathbf{G}_{TT}\boldsymbol{\Lambda}_T \\ &\boldsymbol{\Lambda}_T = \boldsymbol{\Lambda}_{TR} - \bar{\bar{\mu}}\boldsymbol{\Lambda}_N \end{aligned}\right\} \Rightarrow$$

$$\begin{aligned} \mathbf{v}_{TR} = {} & (\mathbf{G}_{TN} - \mathbf{G}_{TT}\bar{\bar{\mu}})\boldsymbol{\Lambda}_N + \mathbf{G}_{TT}\boldsymbol{\Lambda}_{TR} \\ & + \mathbf{E}\boldsymbol{\gamma}_T^- + \mathbf{v}_{TL} \end{aligned} \tag{10}$$

where $\bar{\bar{\mu}} = \mathrm{diag}\{\mu_i\}$, $\bar{\bar{\varepsilon}}_N = \mathrm{diag}\{\varepsilon_{Ni}\}$, i is the index of the impact points, $\mathbf{E}$ the identity matrix, and μ, ε_N, the coefficients of friction and restitution, respectively.

From (6) to (10) an LCP is formulated that treats a frictional multi-impact:

$$\begin{pmatrix} \mathbf{v}_N \\ \mathbf{v}_{TR} \\ \boldsymbol{\Lambda}_{TL} \end{pmatrix} = \begin{pmatrix} \mathbf{G}_{NN} - \mathbf{G}_{NT}\bar{\bar{\mu}} & \mathbf{G}_{NT} & \mathbf{0} \\ \mathbf{G}_{TN} - \mathbf{G}_{TT}\bar{\bar{\mu}} & \mathbf{G}_{TT} & \mathbf{E} \\ 2\bar{\bar{\mu}} & -\mathbf{E} & \mathbf{0} \end{pmatrix} \begin{pmatrix} \boldsymbol{\Lambda}_N \\ \boldsymbol{\Lambda}_{TR} \\ \mathbf{v}_{TL} \end{pmatrix} + \begin{pmatrix} (\bar{\bar{\varepsilon}}_N + \mathbf{E})\boldsymbol{\gamma}_N^- \\ \mathbf{E}\boldsymbol{\gamma}_T^- \\ \mathbf{0} \end{pmatrix} \tag{11}$$

$$\begin{pmatrix} \mathbf{v}_N \\ \mathbf{v}_{TR} \\ \boldsymbol{\Lambda}_{TL} \end{pmatrix} \geq 0 \qquad \begin{pmatrix} \boldsymbol{\Lambda}_N \\ \boldsymbol{\Lambda}_{TR} \\ \mathbf{v}_{TL} \end{pmatrix} \geq 0$$

$$\begin{pmatrix} \mathbf{v}_N \\ \mathbf{v}_{TR} \\ \boldsymbol{\Lambda}_{TL} \end{pmatrix}^T \begin{pmatrix} \boldsymbol{\Lambda}_N \\ \boldsymbol{\Lambda}_{TR} \\ \mathbf{v}_{TL} \end{pmatrix} = 0 \tag{12}$$

As illustrated in later sections, in the form of (11) and (12) the formulated LCP yields a great variety of solutions and is capable of encapsulating different impact states such as "slip", "stick" and reversal of sign, both for single-impact [16] and for double-impact, and contains also impacts of non-impulsive behavior. The adopted approach is thus set-valued and non-smooth in contrast to the commonly adopted, in earthquake engineering literature, contact-element approach (see for example references in [3]). The main difference with the pertinent LCP of [16] that treats single collisions, is that all elements of the LCP (11) are, in the general case, matrices instead of scalar quantities. Similar LCP formulations have been proposed in the past among others by Kwack and Lee [19] and Klarbring and Bjrrkman [20]. The proposed LCP formulation (11) and (12) though, is very well-suited for the needs of the present analysis, which is confined to analytical solutions.

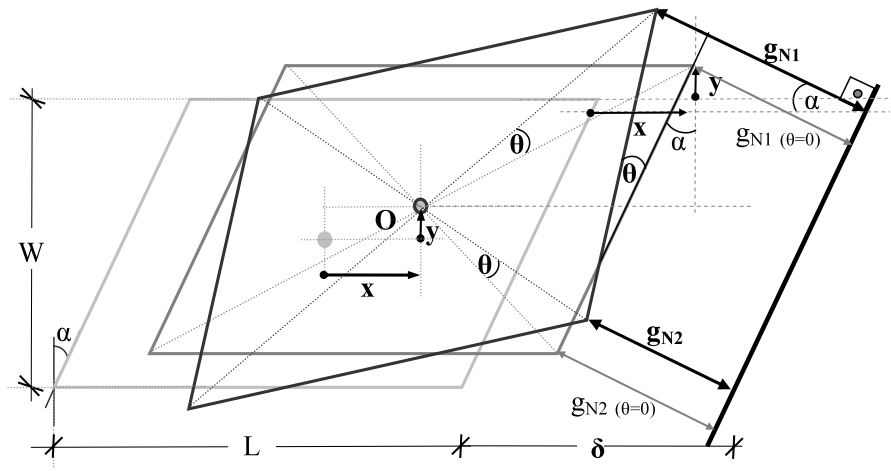

Fig. 4 Relative distance of the two potential impact points for planar translational and rotational motion of a skew bridge segment (rigid body). *Light gray line*—initial position, *dark gray line*—position after translational motion, *black line*—position after rotation

3 Geometric considerations

3.1 The kinematic part of the impact problem

The kinematic part of the impact problem consists in expressing the relative distances g_i (gap functions) and the corresponding velocities γ_i of the (potential) impact points i as a function of the generalized coordinates q_i. The generalized coordinate vector is comprised by the (three) degrees of freedom of a rigid body in plan: two translational (x, y) along the two horizontal axes and one rotational (θ) around the vertical axis; $\mathbf{q}^T = [x\ y\ \theta]$. The pertinent velocities are given by $\dot{\mathbf{q}} = \mathbf{u} = (u_x, u_y, u_\theta)^T$.

Figure 4 presents a skew bridge segment (rigid body) moving in plan against a rigid barrier, which herein is considered as an inelastic half-space. The relative distance of the two potential impact points g_{N1}, g_{N2} can be derived, after some geometric considerations, as:

$$\begin{aligned} g_{N1} &= (\delta - x)\cos\alpha + y\sin\alpha + \frac{1}{2}\big[L\cos a(1-\cos\theta) \\ &\quad + (W/\cos a + L\sin a)\sin\theta\big] \\ g_{N2} &= (\delta - x)\cos\alpha + y\sin\alpha - \frac{1}{2}\big[L\cos a(\cos\theta - 1) \\ &\quad + (W/\cos a - L\sin a)\sin\theta\big] \end{aligned} \tag{13}$$

where δ is the gap width, α the skew angle, L the length and W the width of the rigid body, respectively.

In order to shorten the equations, the following notations are introduced:

$$\begin{aligned} &\mathrm{c}\,a = \cos a \qquad \mathrm{s}\,a = \sin a \qquad r_T = L\,\mathrm{c}\,a/2 \\ &r_1 = (L\,\mathrm{s}\,a + W/\mathrm{c}\,a)/2 \qquad r_2 = (L\,\mathrm{s}\,a - W/\mathrm{c}\,a)/2 \\ &\tilde{r}_{N1} = \frac{1}{2}[L\,\mathrm{c}\,a\sin\theta + 2r_1\cos\theta] \\ &\tilde{r}_{N2} = \frac{1}{2}[L\,\mathrm{c}\,a\sin\theta + 2r_2\cos\theta] \\ &\tilde{r}_{T1} = \frac{1}{2}[-2r_1\sin\theta + L\,\mathrm{c}\,a\cos\theta] \\ &\tilde{r}_{T2} = \frac{1}{2}[2r_2\sin\theta + L\,\mathrm{c}\,a\cos\theta] \end{aligned} \tag{14}$$

Quantities r_1, r_2, and r_T, are the lever arms of the pertinent impulses $\boldsymbol{\Lambda}_1$ and $\boldsymbol{\Lambda}_2$ with respect to the center of mass, under the assumption of small deformations (see Fig. 6 later on). Quantities $\tilde{r}_{N1}$, $\tilde{r}_{N2}$, $\tilde{r}_{T1}$, $\tilde{r}_{T2}$ are the corresponding lever arms in the normal and the transversal direction of the two impacts for large deformations, it follows that: $\tilde{r}_{Ni} \underset{(\theta\to 0)}{\to} r_i$ and $\tilde{r}_{Ti} \underset{(\theta\to 0)}{\to} r_T$ where $i = 1, 2$.

The relative velocities of the two impacts in the longitudinal direction, γ_{N1} and γ_{N2}, are calculated by differentiating in time the expressions of g_{N1} and g_{N2} (13). In the transversal direction the relative velocities, γ_{T1} and γ_{T2}, are derived similarly after calculating the distance variation (e.g. from the initial position—light gray line) due to translational (dark gray line) and rotational (black line) motion with the help of Fig. 4.

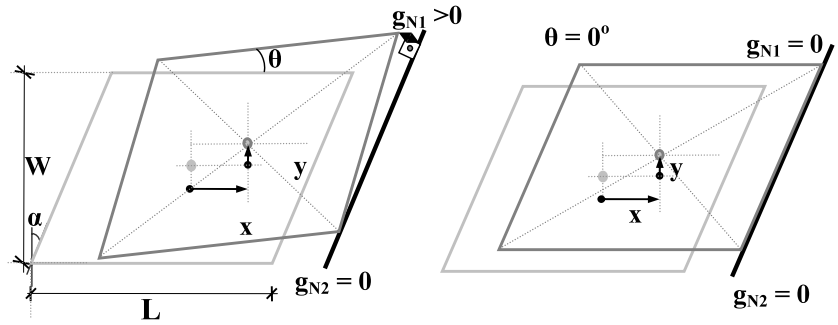

Fig. 5 Single-impact (*left*), and multi-impact (*right*) of a planar skew rigid body

$$
\begin{aligned}
\gamma_{N1} &= \underbrace{(-\mathrm{c}\,a \quad \mathrm{s}\,a \quad \tilde{r}_{N1})}_{\mathbf{w}_{N1}^T} \underbrace{\begin{pmatrix} u_x \\ u_y \\ u_\theta \end{pmatrix}}_{\mathbf{u}} \\
\gamma_{N2} &= \underbrace{(-\mathrm{c}\,a \quad \mathrm{s}\,a \quad \tilde{r}_{N2})}_{\mathbf{w}_{N2}^T} \underbrace{\begin{pmatrix} u_x \\ u_y \\ u_\theta \end{pmatrix}}_{\mathbf{u}} \\
\gamma_{T1} &= \underbrace{(\mathrm{s}\,a \quad \mathrm{c}\,a \quad \tilde{r}_{T1})}_{\mathbf{w}_{T1}^T} \underbrace{\begin{pmatrix} u_x \\ u_y \\ u_\theta \end{pmatrix}}_{\mathbf{u}} \\
\gamma_{T2} &= \underbrace{(\mathrm{s}\,a \quad \mathrm{c}\,a \quad \tilde{r}_{T2})}_{\mathbf{w}_{T2}^T} \underbrace{\begin{pmatrix} u_x \\ u_y \\ u_\theta \end{pmatrix}}_{\mathbf{u}}
\end{aligned}
\tag{15}
$$

3.2 Impact types considered

In skew bridges with deck-abutment joints, impact in plan can take place either in a corner, single (point) impact or along a side multi- (point) impact. In order to cover all potential impact types, from a geometrical point of view, the following cases are distinguished: single-impact (Fig. 5, left) and multi-impact (Fig. 5, right).

4 Frictionless impact

4.1 Single-frictionless impact

Firstly, the case of frictionless impact is discussed without referring to the LCP (11). The effective mass during collision, in the normal direction, G_{NN}^{-1} [21], is calculated as:

$$
G_{NN} \doteq \frac{1}{m} + \tilde{r}_N^2 \frac{1}{I_m} \qquad G_{NN}^{-1} = \frac{m I_m}{I_m + \tilde{r}_N^2 m} \tag{16}
$$

where the lever arm $\tilde{r}_N$ is taken as $\tilde{r}_N = \tilde{r}_{N1}$ or $\tilde{r}_{N2}$ depending on the examined corner where impact takes place and I_m is the inertial mass. The impulse vector $\boldsymbol{\Lambda}_N$ can be estimated according to the assumed impact law, herein Newton's law [21]:

$$
\boldsymbol{\Lambda}_N = -\mathbf{G}_{NN}^{-1}(\mathbf{E} + \bar{\bar{\varepsilon}}_N)\boldsymbol{\gamma}_N^- \tag{17}
$$

where $\mathbf{E}$ is the identity matrix and $\bar{\bar{\varepsilon}}_N = \mathrm{diag}\{\varepsilon_{Ni}\}$ the diagonal matrix comprised by the coefficients of restitution of impacts i.

In the case of single-impact (Fig. 5, left), (17) simplifies to

$$
\begin{aligned}
\Lambda_N &= (1+\varepsilon_N)\,\frac{-m I_m}{I_m + \tilde{r}_N^2 m} \\
&\quad \times \underbrace{(-\mathrm{c}\,a \cdot u_x^- + \mathrm{s}\,a \cdot u_y^- + \tilde{r} \cdot u_\theta^-)}_{\gamma_N^-} \\
&\Leftrightarrow \quad \frac{\Lambda_N}{m\gamma_N^-} = -\frac{1+\varepsilon_N}{1+\frac{\tilde{r}_N^2}{\rho^2}}
\end{aligned}
\tag{18}
$$

ρ is the radius of gyration, defined from $\rho^2 = I_m/m$.

4.2 Multiple frictionless impact

Full-edge impact is modeled (and referred to) as double impact due to rigid body assumption. Double impact occurs (Fig. 5, right) when $\theta^- = 0$ and $u_\theta^- = 0$. Note that pre-impact velocities u_x^-, u_y^- are kept arbitrary. In this case matrix $\mathbf{G}_{NN}$ and its inverse $\mathbf{G}_{NN}^{-1}$ are as follows:

$$\mathbf{G}_{NN} \doteq \begin{pmatrix} \frac{1}{m} + r_1^2 \frac{1}{I_m} & \frac{1}{m} + r_1 r_2 \frac{1}{I_m} \\ \frac{1}{m} + r_2 r_1 \frac{1}{I_m} & \frac{1}{m} + r_2^2 \frac{1}{I_m} \end{pmatrix} \tag{19}$$

$$\mathbf{G}_{NN}^{-1} = \frac{1}{(r_1 - r_2)^2} \begin{pmatrix} I_m + r_2^2 m & -I_m - r_1 r_2 m \\ -I_m - r_2 r_1 m & I_m + r_1^2 m \end{pmatrix}$$

In order to determine the unknown generalized velocities after impact, $\mathbf{u}^+$, one has to calculate first the corresponding impulses $\boldsymbol{\Lambda}_N$. With the aid of Newton's impact law (17) it follows that

$$\boldsymbol{\Lambda}_N = \begin{pmatrix} \Lambda_{N1} \\ \Lambda_{N2} \end{pmatrix} = \frac{-\gamma_N^-}{(r_1 - r_2)^2} \times \begin{pmatrix} I_m(\varepsilon_{N1} - \varepsilon_{N2}) \\ \quad + m(r_2^2 + r_2^2 \varepsilon_{N1} - r_1 r_2 - r_1 r_2 \varepsilon_{N2}) \\ I_m(-\varepsilon_{N1} + \varepsilon_{N2}) \\ \quad + m(-r_1 r_2 - r_1 r_2 \varepsilon_{N1} + r_1^2 + r_1^2 \varepsilon_{N2}) \end{pmatrix} \tag{20}$$

Assuming the coefficients of restitution in the two impacts $\varepsilon_{N1}, \varepsilon_{N2}$ are the same $\varepsilon_{N1} = \varepsilon_{N2} = \varepsilon_N$ (20) yields

$$\begin{pmatrix} \frac{\Lambda_{N1}}{m\gamma_N^-} \\ \frac{\Lambda_{N2}}{m\gamma_N^-} \end{pmatrix} = -(1+\varepsilon_N) \begin{pmatrix} -\frac{r_2}{r_1 - r_2} \\ \frac{r_1}{r_1 - r_2} \end{pmatrix} = -\frac{(1+\varepsilon_N)}{2} \begin{pmatrix} 1 - \frac{\sin a \cos a}{W/L} \\ 1 + \frac{\sin a \cos a}{W/L} \end{pmatrix} \tag{21}$$

Using (4) the unknown generalized velocities after impact $\mathbf{u}^+$ are calculated as

$$\mathbf{u}^+ = \mathbf{u}^- - \mathbf{M}^{-1}\mathbf{W}_N \underbrace{\mathbf{G}_N^{-1}(\mathbf{E} + \bar{\bar{\varepsilon}}_N)\boldsymbol{\gamma}^-}_{-\boldsymbol{\Lambda}_N}$$

$$\Rightarrow \begin{pmatrix} u_x^+ \\ u_y^+ \\ u_\theta^+ \end{pmatrix} = \begin{pmatrix} u_x^- \\ u_y^- \\ 0 \end{pmatrix} + \begin{pmatrix} -\frac{\mathrm{c}a}{m}\Lambda_{N1} - \frac{\mathrm{c}a}{m}\Lambda_{N2} \\ \frac{\mathrm{s}a}{m}\Lambda_{N1} + \frac{\mathrm{s}a}{m}\Lambda_{N2} \\ \frac{r_1}{I_m}\Lambda_{N1} + \frac{r_2}{I_m}\Lambda_{N2} \end{pmatrix} \tag{22}$$

From (22), due to (21), it follows that the post-impact angular velocity is zero, $u_\theta^+ = 0$.

Impulses Λ_{N1} and Λ_{N2} are given by (21) as a function of the geometry (α, L, W), the coefficient of restitution in the normal direction ε_N, and the translational mass m. However, (21) are incomplete without the physical inequality constraint $\Lambda_N \geq 0$, which accounts for the unilateral nature of impact. Unlike single impact (18), in multi-impacts the satisfaction of the inequality constraint demands special attention [21].

Indeed, taking into account that by definition: $m(1+\varepsilon_N) > 0$, and that in order for contact to occur the relative velocity must be negative $\gamma_N^- \leq 0$ (approach process), the sign of impulse depends solely on the (proposed) dimensionless criterion, η_0, which relates the ratio of the two sides in plan (L, W) with the skew angle, α, as follows:

$$\eta_0 = \frac{\sin 2a}{2(W/L)} \tag{23}$$

For $\eta_0 > 1$, impulse at the acute corner according to (21) is negative $\Lambda_{N1} < 0$, which lacks physical interpretation. On the contrary, impulse at the obtuse corner is always positive, $\Lambda_{N2} > 0$ (21).

As mentioned previously, no angular velocity is developed after the examined oblique impact (Fig. 5, right) and thus rotation remains zero, $u_\theta^+ = 0$, as assumed before impact. This not so intuitive conclusion though, is valid only when constraint $\Lambda_N \geq 0$ is satisfied or equivalently when $\eta_0 < 1$ (Fig. 6, top). If $\eta_0 > 1$ (Fig. 6, bottom), contact at the acute corner must be ignored (since $\Lambda_{N1} < 0$) and (22) of the multi-impact have to be replaced by (18), assuming single impact solely at the obtuse corner. In summary, the generalized angular velocity, u_θ^+ , after double impact is given by:

$$u_\theta^+ = \begin{cases} \frac{\gamma_N^-}{r_2} \frac{1+\varepsilon_N}{(\frac{\rho}{r_2})^2+1}, & \text{if } \eta_0 = \frac{\sin 2a}{2(W/L)} > 1 \\ 0, & \text{if } \eta_0 = \frac{\sin 2a}{2(W/L)} < 1 \end{cases} \tag{24}$$

Equations (24) unveil two distinct response patterns of a planar skew body after double oblique impact. When $\eta_0 < 1$, or equivalently $W/\cos\alpha > L\sin\alpha$ (Fig. 6, top), the angular momentums of the two impulses Λ_{N1} and Λ_{N2} with respect to the center of mass (C.M.) are in different directions and cancel out, as a consequence no angular velocity is developed (24). On the contrary, when $\eta_0 > 1$, subsequently $W/\cos\alpha < L\sin\alpha$ (Fig. 6, bottom) the angular mo-

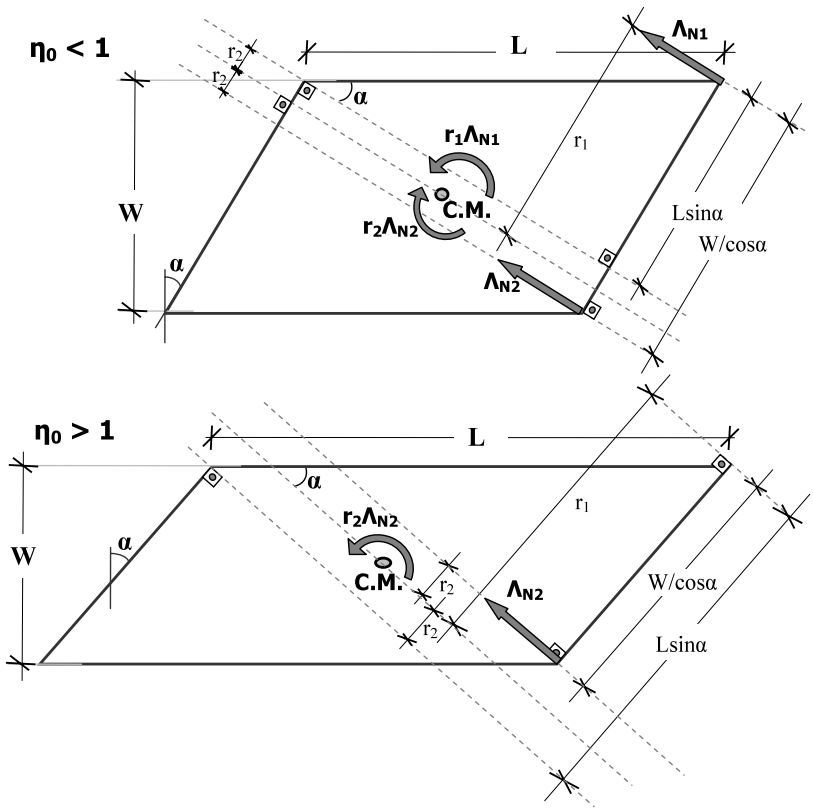

Fig. 6 Geometrical interpretation of the rotational mechanism of skew bridges (frictionless impact). *Top*: no rotation is developed after double impact. *Bottom*: double-impact results in rotation

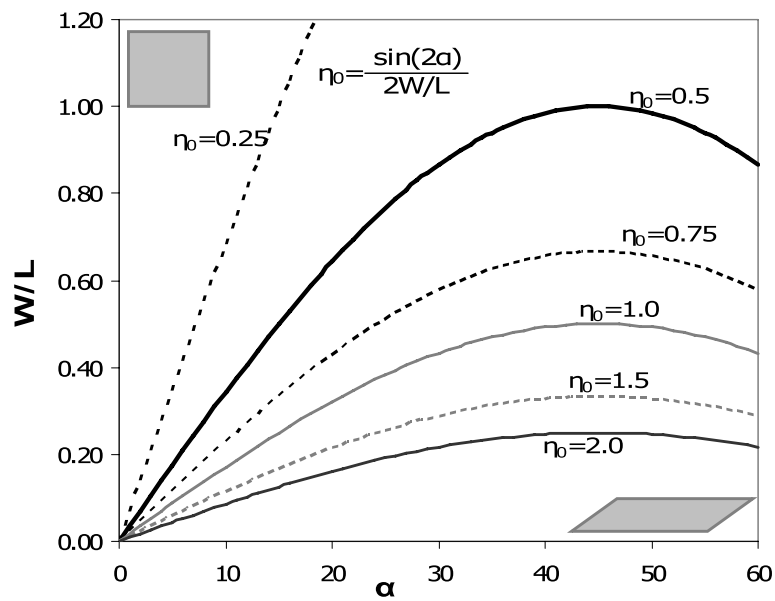

Fig. 7 Contours of the dimensionless skew criterion η_0 values in the plane: width/length (W/L)–skew angle (α)

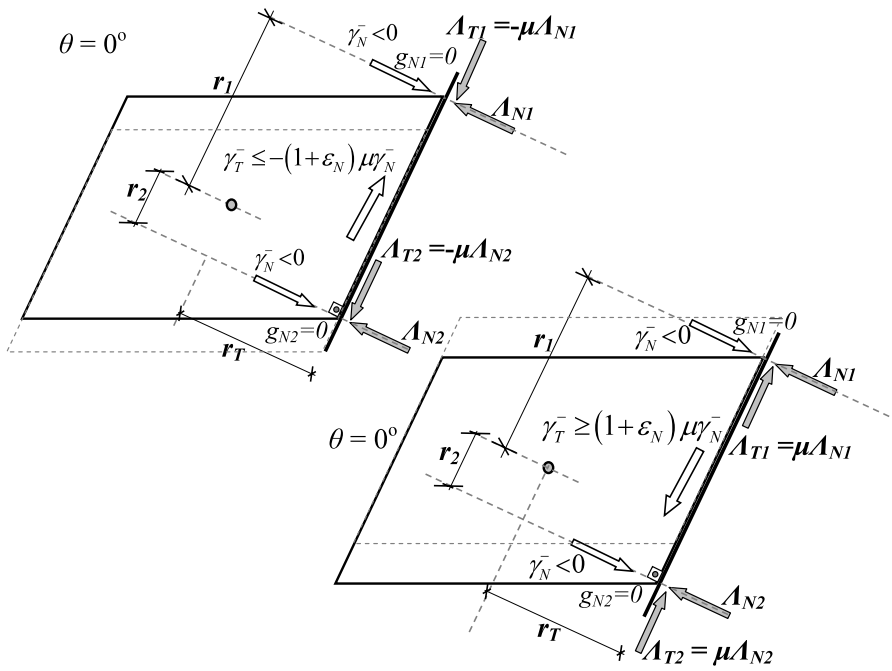

Fig. 8 Double backward slip (*top*), double forward slip (*bottom*)

mentums of the two impulses Λ_{N1} and Λ_{N2} are in the same direction, the impulse at the acute corner should then be neglected since according to (21) it changes sign ($\Lambda_{N1} < 0$) and angular velocity is developed (24). This behavior of a skew rigid body after double oblique impact is reminiscent of the behavior of the double impact of a rod [21].

To date, these two distinct response patterns of deck-abutment collisions of skew bridges were not known. Furthermore, (24) reveal that the tendency of such bridges towards rotation (and most importantly unseating) is not a factor of the skew angle (α) alone, as considered in empirical vulnerability methodologies e.g. [7] but rather of the overall geometry of the body in-plan (criterion η_0 (23)). Figure 7 plots contours of the dimensionless criterion η_0 on the plane: width and length ratio (W/L) vs. skew angle (α). Every point on this plane shapes the form of a skew bridge segment in plan. For example, small α and W/L ratio around unity correspond to a square body (Fig. 7, top left, $\eta_0 \approx 0.2$) while large α and low W/L ratios to a bridge like the one at the bottom right of Fig. 7 ($\eta_0 \approx 2.0$). Figure 7 also shows that a bridge with a smaller skew angle (α) is feasible to yield a greater dimensionless skew value (η_0) than one with a larger skew angle.

5 Frictional impact

A more realistic description of the oblique impact response of skew bridges is obtained when friction is taken into account. However, the ad hoc method, of checking the sign of the impulse a posteriori used in the previous section, is inappropriate for complicated (such as multi-frictional) impact configurations [16, 21]. Instead, a more effective method is to formulate the impact problem taking into account the unilateral character of contact from the beginning, for instance by means of a Linear Complementarity Problem (LCP, (11) and (12)).

The LCP (11) with the complementarity conditions (12) yields a great variety of solutions. In addition to the single-impact states investigated in [16] three multi-impact states appear: double backward slip (Fig. 8, top), double forward slip (Fig. 8, bottom) and double stick (Fig. 9, later on). It is reminded that in the transversal direction a Coulomb friction model is realized via a set-value force law; the Sgn(x) function (Fig. 3).

5.1 Multiple frictional impact states

The discussion of frictional impact begins with double impact. Later in the paper, it is shown that for the

mechanical configuration considered herein, single-impact states can be seen as a special case of the double impact examined. Double impact occurs when $u_\theta^- = 0$ and $\theta^- = 0$ (Fig. 5, right).

Firstly, **G**-matrices are calculated according to (6):

$$\begin{aligned}
\mathbf{G}_{NN} &= \begin{pmatrix} \frac{1}{m} + \frac{r_1^2}{I_m} & \frac{1}{m} + \frac{r_1 r_2}{I_m} \\ \frac{1}{m} + \frac{r_1 r_2}{I_m} & \frac{1}{m} + \frac{r_2^2}{I_m} \end{pmatrix} \\
\mathbf{G}_{NT} &= \begin{pmatrix} \frac{r_1 r_T}{I_m} & \frac{r_1 r_T}{I_m} \\ \frac{r_2 r_T}{I_m} & \frac{r_2 r_T}{I_m} \end{pmatrix} \\
\mathbf{G}_{TT} &= \begin{pmatrix} \frac{1}{m} + \frac{r_T^2}{I_m} & \frac{1}{m} + \frac{r_T^2}{I_m} \\ \frac{1}{m} + \frac{r_T^2}{I_m} & \frac{1}{m} + \frac{r_T^2}{I_m} \end{pmatrix} \\
\mathbf{G}_{TN} &= \begin{pmatrix} \frac{r_1 r_T}{I_m} & \frac{r_2 r_T}{I_m} \\ \frac{r_1 r_T}{I_m} & \frac{r_2 r_T}{I_m} \end{pmatrix}
\end{aligned} \tag{25}$$

The inverse of matrix $\mathbf{G}_{NN}$ expresses the effective mass in the normal direction of the impact [21] and is given by

$$\mathbf{G}_{NN}^{-1} = \frac{1}{(r_1 - r_2)^2} \begin{pmatrix} I_m + r_2^2 m & -I_m - r_1 r_2 m \\ -I_m - r_2 r_1 m & I_m + r_1^2 m \end{pmatrix} \tag{26}$$

On the contrary, matrices $\mathbf{G}_{NT}$, $\mathbf{G}_{TT}$ and $\mathbf{G}_{TN}$ are not invertible since determinants: $|\mathbf{G}_{NT}| = |\mathbf{G}_{TT}| = |\mathbf{G}_{TN}| = 0$ are zero. This is a typical case of dependent constraints which arises because the two impacts are linearly interdependent in the transversal direction. Such *overconstrained* problems appear often in multibody dynamics with multi-impacts and several ways of treating them have been proposed in the literature [14].

5.1.1 Double backward slip (Fig. 8, top)

The complementarity conditions (12) for $\Lambda_{N1} > 0$, $\Lambda_{N2} > 0$, $\Lambda_{T1} = +\mu\Lambda_{N1}$ and $\Lambda_{T2} = +\mu\Lambda_{N2}$ yield: $v_{N1} = 0$, $v_{N2} = 0$, $\Lambda_{TR1} = 2\mu\Lambda_{N1}$, $v_{TR1} = 0$, $\Lambda_{TR2} = 2\mu\Lambda_{N2}$ and $v_{TR2} = 0$. Thus, (9) reduces to

$$(\mathbf{G}_{NN} + \mathbf{G}_{NT}\bar{\bar{\mu}})\boldsymbol{\Lambda}_N = -(\bar{\bar{\varepsilon}}_N + \mathbf{E})\boldsymbol{\gamma}_N^- \tag{27}$$

The inverse of matrix $(\mathbf{G}_{NN} + \mathbf{G}_{NT}\bar{\bar{\mu}})$ is given by

$$\begin{aligned}
(\mathbf{G}_{NN} + \mathbf{G}_{NT}\bar{\bar{\mu}})^{-1} &= \frac{1}{(r_1 - r_2)^2} \\
&\times \begin{pmatrix} I_m + m(r_2^2 + \mu r_2 r_T) & -I_m - m(r_1 r_2 + \mu r_1 r_T) \\ -I_m - m(r_1 r_2 + \mu r_2 r_T) & I_m + m(r_1^2 + \mu r_1 r_T) \end{pmatrix}
\end{aligned} \tag{28}$$

Note that for $\mu = 0$ (28) reduces to (19) of frictionless collisions. The impulse vector is derived from (27) due to (28) as:

$$\begin{pmatrix} \frac{\Lambda_{N1}}{m\gamma_N^-} \\ \frac{\Lambda_{N2}}{m\gamma_N^-} \end{pmatrix} = -(1 + \varepsilon_N) \begin{pmatrix} \frac{-r_2 - \mu r_T}{r_1 - r_2} \\ \frac{r_1 + \mu r_T}{r_1 - r_2} \end{pmatrix} \tag{29}$$

Equation (10), replacing $\boldsymbol{\Lambda}_N$ from (29), becomes

$$\begin{aligned}
\mathbf{v}_{TL} &= (\mathbf{G}_{TN} + \mathbf{G}_{TT}\bar{\bar{\mu}})(\mathbf{G}_{NN} + \mathbf{G}_{NT}\bar{\bar{\mu}})^{-1} \\
&\times (\bar{\bar{\varepsilon}}_N + \mathbf{E})\boldsymbol{\gamma}_N^- - \mathbf{E}\boldsymbol{\gamma}_T^-
\end{aligned} \tag{30}$$

The product $(\mathbf{G}_{TN} + \mathbf{G}_{TT}\bar{\bar{\mu}})(\mathbf{G}_{NN} + \mathbf{G}_{NT}\bar{\bar{\mu}})^{-1}$ after some algebra simplifies to

$$\begin{aligned}
&(\mathbf{G}_{TN} + \mathbf{G}_{TT}\bar{\bar{\mu}})(\mathbf{G}_{NN} + \mathbf{G}_{NT}\bar{\bar{\mu}})^{-1} \\
&= \begin{pmatrix} -\frac{\mu r_2 - r_T}{r_1 - r_2} & \frac{\mu r_1 - r_T}{r_1 - r_2} \\ -\frac{\mu r_2 - r_T}{r_1 - r_2} & \frac{\mu r_1 - r_T}{r_1 - r_2} \end{pmatrix}
\end{aligned} \tag{31}$$

Replacing (31) in (30) shows that the transversal post-impact velocities of the two impact points, in the case of double backward slip, are equal:

$$\gamma_{T1}^+ = \gamma_{T2}^+ \qquad \frac{\gamma_{T1}^+}{\gamma_N^+} = -\frac{1 + \varepsilon_N}{\varepsilon_N}\mu + \frac{1}{\varepsilon_N}\frac{\gamma_T^-}{\gamma_N^-} \tag{32}$$

According to the Newton–Euler equations double backward slip results in zero angular velocity, since

$$\begin{aligned}
&\mathbf{M}(\mathbf{u}^+ - \mathbf{u}^-) = \mathbf{W}_N\boldsymbol{\Lambda}_N + \mathbf{W}_T\boldsymbol{\Lambda}_T \\
&\Rightarrow \quad I_m(u_\theta^+ - 0) = r_1\Lambda_{N1} + r_2\Lambda_{N2} \\
&\qquad\qquad + r_T(\Lambda_{T1} + \Lambda_{T2}) \\
&\qquad\qquad = 0 \quad \Rightarrow \quad u_\theta^+ = 0
\end{aligned}$$

Double backward slip (Fig. 8, top) occurs when: $(\boldsymbol{\Lambda}_N\ \boldsymbol{\Lambda}_{TR}\ \mathbf{v}_{TL})^T \geq 0 \ \Rightarrow\ (\Lambda_{N1}\ \Lambda_{N2}\ \Lambda_{TR1}\ \Lambda_{TR2}\ v_{TL1}\ v_{TL2})^T \geq 0$, which with the help of the LCP (11) yield two existential conditions:

$$\begin{aligned}
&\Lambda_{N1} \geq 0 \quad \Rightarrow \quad r_2 + \mu r_T \leq 0 \quad \Rightarrow \quad \eta_1 \leq 1 \\
&\text{where } \eta_1 \doteq \eta_0\left(1 + \frac{\mu}{\tan a}\right)
\end{aligned} \tag{33}$$

$$\mathbf{v}_{TL} \geq 0 \quad \Rightarrow \quad \frac{\gamma_{T1}^-}{\gamma_N^-} \geq (1+\varepsilon_N)\mu \quad \text{and} \quad \gamma_{T1}^- = \gamma_{T2}^- \tag{34}$$

5.1.2 Double forward slip (Fig. 8, bottom)

Following the same reasoning for forward slip ($\Lambda_{N1} > 0$, $\Lambda_{N2} > 0$, $\Lambda_{T1} = -\mu\Lambda_{N1}$ and $\Lambda_{T2} = -\mu\Lambda_{N2}$), as for double backward slip, the normal impulse vector, $\boldsymbol{\Lambda}_N$ is given by

$$\begin{pmatrix} \frac{\Lambda_{N1}}{m\gamma_N^-} \\ \frac{\Lambda_{N2}}{m\gamma_N^-} \end{pmatrix} = -(1+\varepsilon_N) \begin{pmatrix} \frac{-r_2+\mu r_T}{r_1-r_2} \\ \frac{r_1-\mu r_T}{r_1-r_2} \end{pmatrix} \tag{35}$$

Equation (10) yields:

$$\mathbf{v}_{TR} = (\mathbf{G}_{TN} - \mathbf{G}_{TT}\bar{\bar{\mu}})(\mathbf{G}_{NN} - \mathbf{G}_{NT}\bar{\bar{\mu}})^{-1} \times (\bar{\bar{\varepsilon}}_N + \mathbf{E})\boldsymbol{\gamma}_N^- + \mathbf{E}\boldsymbol{\gamma}_T^- \tag{36}$$

and after evaluating the product

$$(\mathbf{G}_{TN} - \mathbf{G}_{TT}\bar{\bar{\mu}})(\mathbf{G}_{NN} - \mathbf{G}_{NT}\bar{\bar{\mu}})^{-1} = \begin{pmatrix} \frac{\mu r_2 + r_T}{r_1 - r_2} & \frac{-\mu r_1 - r_T}{r_1 - r_2} \\ \frac{\mu r_2 + r_T}{r_1 - r_2} & \frac{-\mu r_1 - r_T}{r_1 - r_2} \end{pmatrix} \tag{37}$$

the post-impact velocities of the two impacts are derived:

$$\gamma_{T1}^+ = \gamma_{T2}^+ \qquad \frac{\gamma_{T1}^+}{\gamma_N^+} = \frac{1+\varepsilon_N}{\varepsilon_N}\mu + \frac{1}{\varepsilon_N}\frac{\gamma_T^-}{\gamma_N^-} \tag{38}$$

Similarly to double backward slip, the post-impact angular velocity is zero.

Double forward slip occurs when $(\boldsymbol{\Lambda}_N \ \boldsymbol{\Lambda}_{TL} \ \mathbf{v}_{TR})^T \geq 0$, and with the help of the LCP (11) the following existential conditions are derived:

$$\left.\begin{aligned} \Lambda_{N1} \geq 0 \quad \Rightarrow \quad \mu r_T \geq r_2 \quad \Rightarrow \quad \eta_0\left(1 - \frac{\mu}{\tan a}\right) \leq 1 \\ \Lambda_{N2} \geq 0 \quad \Rightarrow \quad r_1 \geq \mu r_T \quad \Rightarrow \quad \eta_0\left(\frac{\mu}{\tan a} - 1\right) \leq 1 \end{aligned}\right\} \Rightarrow \quad |\eta_2| \leq 1 \quad \text{where } \eta_2 \doteq \eta_0\left(1 - \frac{\mu}{\tan a}\right) \tag{39}$$

$$\mathbf{v}_{TR} \geq 0 \quad \Rightarrow \quad \frac{\gamma_T^-}{\gamma_N^-} \leq (1+\varepsilon_N)\mu \quad \text{and} \quad \gamma_{T1}^- = \gamma_{T2}^- \tag{40}$$

5.1.3 Double stick

The complementarity conditions (12) for $\Lambda_{N1} > 0$, $\Lambda_{N2} > 0$, $|\Lambda_{T1}| > \mu\Lambda_{N1}$ and $|\Lambda_{T2}| < \mu\Lambda_{N2}$ yield: $v_{N1} = 0$, $v_{N2} = 0$, $\Lambda_{TR1} > 0$, $\Lambda_{TR2} > 0$, $v_{TR1} = 0$, $v_{TR2} = 0$, $\Lambda_{TL1} > 0$, $\Lambda_{TL2} > 0$, $v_{TL1} = 0$, and $v_{TL2} = 0$. Thus, (9) and (10) yield a system of coupled equations that must be solved for both unknown vectors $\boldsymbol{\Lambda}_N$ and $\boldsymbol{\Lambda}_{TR}$ simultaneously:

$$\begin{aligned} \mathbf{0} &= (\mathbf{G}_{NN} - \mathbf{G}_{NT}\bar{\bar{\mu}})\boldsymbol{\Lambda}_N + \mathbf{G}_{NT}\boldsymbol{\Lambda}_{TR} + (\bar{\bar{\varepsilon}}_N + \mathbf{E})\boldsymbol{\gamma}_N^- \\ \mathbf{0} &= (\mathbf{G}_{TN} - \mathbf{G}_{TT}\bar{\bar{\mu}})\boldsymbol{\Lambda}_N + \mathbf{G}_{TT}\boldsymbol{\Lambda}_{TR} + \mathbf{E}\boldsymbol{\gamma}_T^- \end{aligned} \tag{41}$$

As mentioned previously matrices $\mathbf{G}_{NT}, \mathbf{G}_{TT}$ and $(\mathbf{G}_{TN} - \mathbf{G}_{TT}\bar{\bar{\mu}})$ are not invertible, since the two impacts are dependent (constraints), thus system (41) has no unique solution. In order to derive a closed-form solution for this type of impact (double stick) the problem can be reformulated.

In the case of double stick the post-impact kinematic state of the rigid body is fully determined by definition: $\mathbf{v}_N = \mathbf{0}$ and $\mathbf{v}_T = \mathbf{0}$. This allows the determination of an equivalent single (point) impact that bypasses the problem of overconstrained impacts. With reference to Fig. 9 the direction vectors of the equivalent impact are

$$\mathbf{w}_N^T = (-\mathrm{c}\,a \quad \mathrm{s}\,a \quad r^*) \qquad \mathbf{w}_T^T = (\mathrm{s}\,a \quad \mathrm{c}\,a \quad r_T) \tag{42}$$

The only unknown under determination is the lever arm of the singe impact in the normal direction r^*. The Newton–Euler equations for the two simulations of impact (double and equivalent single, Fig. 9) give:

$$\mathbf{W}_N\boldsymbol{\Lambda}_N + \mathbf{W}_T\boldsymbol{\Lambda}_T = W_N\Lambda_N + W_T\Lambda_T \tag{43}$$

The left-hand side of (43) is the matrix expression of impulse under the assumption of double impact (Fig. 9, top), while the right-hand side the corresponding scalar impulse of the equivalent single impact (Fig. 9, bottom). Since the post-impact kinematic state of the body is known by assumption, it follows that the product $\mathbf{M}(\mathbf{u}^+ - \mathbf{u}^-)$ is also known. After some algebra (43) yields:

$$\begin{aligned} &\Lambda_{N1} + \Lambda_{N2} = \Lambda_N \\ &\Lambda_{T1} + \Lambda_{T2} = \Lambda_T \\ &r_1\Lambda_{N1} + r_2\Lambda_{N2} = r^*\Lambda_N \end{aligned} \tag{44}$$

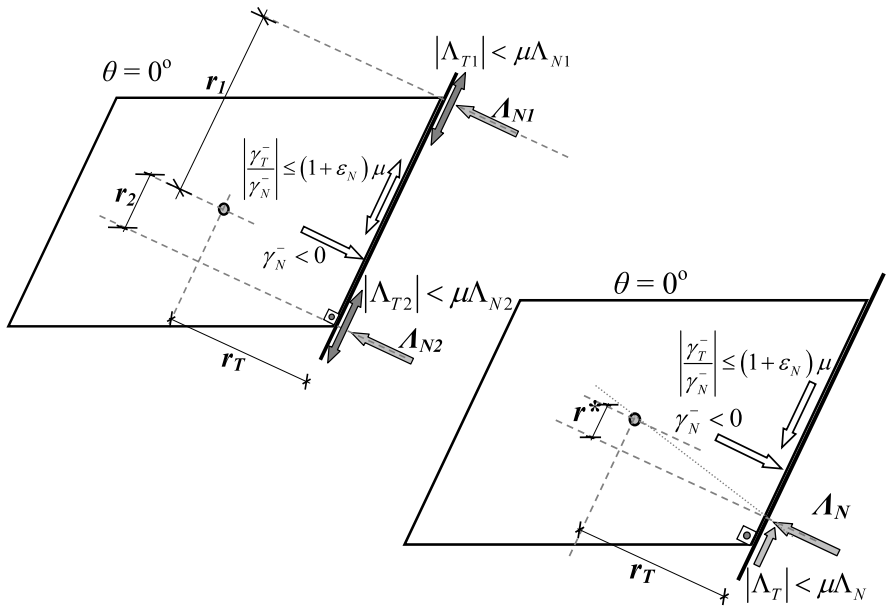

Fig. 9 Double stick, simulated as multi-impact (*left*) and single impact (*right*)

The first two equations of (44) stand for the linear momentum equivalence between the two (double and single) impacts, while the third equation of (44), expresses the equivalence of angular momentums.

The unknown lever of the single impact, in the normal direction, is given as a function of the pre-impact velocities and the coefficient of restitution from (5) due to (43), after some algebra, as:

$$r^* = -\frac{\Lambda_T}{\Lambda_N} r_T = \frac{-1}{1+\varepsilon_N} \frac{\gamma_T^-}{\gamma_N^-} r_T \tag{45}$$

Hence introducing condition (45) an equivalent single impact with the examined double stick may be completely determined a priori.

In order to derive the existential conditions of double stick, impulses Λ_{N1} and Λ_{N2} are first calculated from (44) introducing condition (45):

$$\Lambda_{N1} = \frac{r^* - r_2}{r_1 - r_2} \Lambda_N \qquad \Lambda_{N2} = \frac{r_1 - r^*}{r_1 - r_2} \Lambda_N \tag{46}$$

Both Λ_{N1} and Λ_{N2} are positive by assumption, hence

$$r_1 \geq r^* \geq r_2 \tag{47}$$

Also by assumption, it holds that: $|\Lambda_T| < \mu \Lambda_N$ which due to (45) gives

$$|r^*/r_T| \leq \mu \tag{48}$$

as well as

$$-\mu(1+\varepsilon_N) \leq \frac{\gamma_T^-}{\gamma_N^-} \leq \mu(1+\varepsilon_N) \tag{49}$$

In addition to condition (49) the following existential conditions arise from (47) with the help of (48):

$$\begin{cases} r_2 - \mu r_T < 0 \\ r_1 + \mu r_T > 0 \end{cases} \Rightarrow \begin{cases} \eta_0(1 - \mu/\tan\alpha) < 1 \\ \eta_0(1 + \mu/\tan\alpha) > 1 \end{cases}$$

$$\Rightarrow \begin{cases} \eta_2 < 1 \\ \eta_1 > 1 \end{cases} \tag{50}$$

When $\Lambda_N = 0$ holds at both impact points, double impacts lack physical interpretation. Hence, the remaining physically feasible combinations of the LCP (11) treat double-impact states during which only one of the two impact points presents a compressive impulse ($\Lambda_N > 0$). The comparison of the following impact states with those considered in [16] reveals that these impacts can be treated also with a similar LCP treating single-frictional impacts.

5.1.4 Backward slip at the obtuse corner

Equations (9) and (10) due to the complementarity conditions (12) and $\Lambda_{N2} > 0$, $\Lambda_{N1} = 0$, and $\Lambda_{T2} = +\mu\Lambda_{N2}$ yield

$$\begin{cases} \frac{\Lambda_{N2}}{m\gamma_N^-} = -\frac{(1+\varepsilon_N)}{1+\frac{r_2^2+\mu r_2 r_T}{\rho^2}} \\ \frac{\gamma_{N1}^+}{\gamma_N^-} = 1+(1+\varepsilon_N)\frac{\rho^2+r_1 r_2+\mu r_1 r_T}{\rho^2+r_2^2+\mu r_2 r_T} \end{cases} \tag{51}$$

The pertinent existential conditions are

$$\begin{cases} \Lambda_{N2} \geq 0 \quad \Rightarrow \quad \rho^2+r_2^2+\mu r_2 r_T \geq 0 \\ v_{N1} \geq 0 \quad \Rightarrow \quad r_2+\mu r_T \leq 0 \Rightarrow \eta_1 \leq 1 \end{cases} \text{ and} \tag{52}$$

$$v_{TL2} \geq 0 \quad \Rightarrow \quad \frac{\gamma_T^-}{\gamma_N^-} \geq (1+\varepsilon_N)\frac{\mu(\rho^2+r_T^2)+r_2 r_T}{\rho^2+r_2^2+\mu r_2 r_T}$$

5.1.5 Backward slip at the acute corner

In the case of backward slip at the acute corner ($\Lambda_{N1} > 0$, $\Lambda_{N2} = 0$, and $\Lambda_{T1} = +\mu\Lambda_{N1}$) the existential conditions are derived, following the same reasoning, as:

$$\begin{cases} \Lambda_{N1} \geq 0 \quad \Rightarrow \quad \mu r_1 r_T + r_1^2 + \rho^2 \geq 0 \\ v_{N2} \geq 0 \quad \Rightarrow \quad (r_1+\mu r_T)(r_1-r_2) \leq 0 \end{cases} \tag{53}$$

It is interesting to note that condition $v_{N2} \geq 0$ results in a contradiction, since both $r_1 - r_2 > 0$ and $r_1 + \mu r_T > 0$ are positive. Hence, single backward slip cannot take place at the acute corner of a skew rigid body, a conclusion not so intuitive.

5.1.6 Forward slip at the obtuse corner

Similarly to backward slip at the obtuse corner, forward slip at the obtuse corner ($\Lambda_{N2} > 0$, $\Lambda_{N1} = 0$, and $\Lambda_{T2} = -\mu\Lambda_{N2}$) results in:

$$\begin{cases} \frac{\Lambda_{N2}}{m\gamma_N^-} = -\frac{(1+\varepsilon_N)}{1+\frac{r_2^2-\mu r_2 r_T}{\rho^2}} \\ \frac{\gamma_{N1}^+}{\gamma_N^-} = 1-(1+\varepsilon_N)\frac{\rho^2+r_1 r_2-\mu r_1 r_T}{\rho^2+r_2^2-\mu r_2 r_T} \end{cases} \tag{54}$$

with the pertinent existential conditions given by

$$\begin{cases} v_{N1} \geq 0 \quad \Rightarrow \quad r_2-\mu r_T \geq 0 \quad \Rightarrow \quad \eta_1 \leq 1 \\ \Lambda_{N2} \geq 0 \quad \Rightarrow \quad \rho^2+r_2^2-\mu r_2 r_T \geq 0 \end{cases} \text{ and} \tag{55}$$

$$v_{TR2} \geq 0 \quad \Rightarrow \quad \frac{\gamma_T^-}{\gamma_N^-} \leq \frac{r_2 r_T-\mu(r_T^2+\rho^2)}{\rho^2+r_2^2-\mu r_2 r_T}(1+\varepsilon_N)$$

5.1.7 Forward slip at the acute corner

Forward slip at the acute corner is described by (54) and (55) substituting lever r_2 with lever r_1 (with the exception of product $r_1 r_2$ which remains as it is).

5.1.8 Stick at the obtuse corner

Impulses in the normal and the transversal direction for stick at the obtuse corner ($\Lambda_{N2} > 0$, $\Lambda_{N1} = 0$, and $|\Lambda_{T2}| < \mu\Lambda_{N2}$) are calculated from (9) and (10) with the help of the complementarity conditions (12) as:

$$\begin{aligned} \frac{\Lambda_{N2}}{m\gamma_N^-} &= \frac{-(\rho^2+r_T^2)(1+\varepsilon_N)+r_2 r_T(1+\varepsilon_T)\frac{\gamma_T^-}{\gamma_N^-}}{\rho^2+r_2^2+r_T^2} \\ \frac{\Lambda_{T2}}{m\gamma_N^-} &= \frac{r_2 r_T(1+\varepsilon_N)-(\rho^2+r_2^2)(1+\varepsilon_T)\frac{\gamma_T^-}{\gamma_N^-}}{\rho^2+r_2^2+r_T^2} \end{aligned} \tag{56}$$

the existential conditions for stick at the obtuse corner are

$$\begin{aligned} &\frac{\gamma_T^-}{\gamma_N^-} < \frac{\rho^2+r_T^2}{r_2 r_T}\frac{1+\varepsilon_N}{1+\varepsilon_T} \\ &\left(\rho^2+r_2^2-\mu r_2 r_T\right)\frac{\gamma_T^-}{\gamma_N^-} > \left[r_2 r_T-\mu\left(\rho^2+r_T^2\right)\right] \times \frac{1+\varepsilon_N}{1+\varepsilon_T} \\ &\left(\rho^2+r_2^2+\mu r_2 r_T\right)\frac{\gamma_T^-}{\gamma_N^-} < \left[r_2 r_T+\mu\left(\rho^2+r_T^2\right)\right] \times \frac{1+\varepsilon_N}{1+\varepsilon_T} \end{aligned} \tag{57}$$

5.1.9 Stick at the acute corner

For (single) stick at the acute corner (56) and (57) hold where in lieu of lever r_2, lever r_1 is used.

The combinations of the LCP (11) with transversal impulses of opposite sign (at the two impacts) lack physical interpretation. If for instance $\Lambda_{T1} = +\mu\Lambda_{N1}$ and $\Lambda_{T2} = -\mu\Lambda_{N2}$ the complementarity conditions (12) yield: $v_{TL1} \geq 0$ and $v_{TR2} \geq 0$.

5.2 Synopsis

The synopsis of all physically feasible combinations of the LCP (11) shows that the response of the examined oblique frictional multi-impact is mainly determined by two criteria: the first criterion is the transversal and the normal velocity ratio γ_T^-/γ_N^- which determines whether the double impact is forward/backward slip or stick. The second criterion is the dimensionless geometrical ratio (η_0) proposed for frictionless impact or the pertinent ratios of frictional impact ($\eta_{1,2}$), given by:

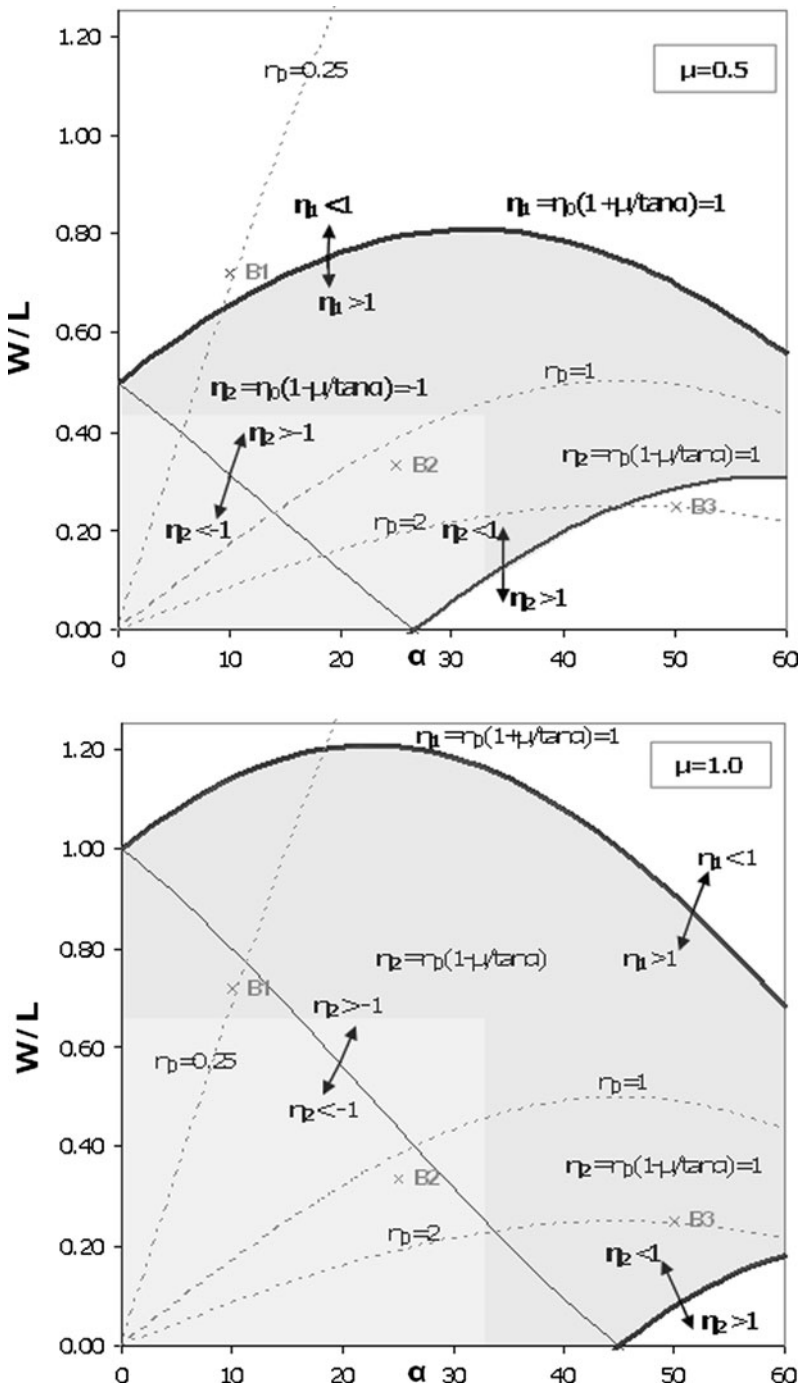

Fig. 10 Critical curves $\eta_0 = 1$, $\eta_1 = 1$, $\eta_2 = \pm 1$ in the plane: width/length (W/L)–skew angle (α), for friction coefficient $\mu = 0.5$ (*top*) and $\mu = 1.0$ (*bottom*)

$$\eta_{1,2} = \eta_0\left(1 \pm \frac{\mu}{\tan a}\right) = \frac{\sin 2a}{2(W/L)}\left(1 \pm \frac{\mu}{\tan a}\right) \quad (58)$$

where sign $(+)$ holds for backward slip (η_1) and sign $(-)$ for forward slip (η_2).

In Fig. 10 the critical curves for both backward $(\eta_1 = 1)$ and forward slip $(\eta_2 = \pm 1)$ are illustrated for a given coefficient of friction $\mu = 0.5$ (top) and $\mu = 1.0$ (bottom). Points B1, B2 and B3 correspond to skew bridges with increasing skew ratios η_0 (see also

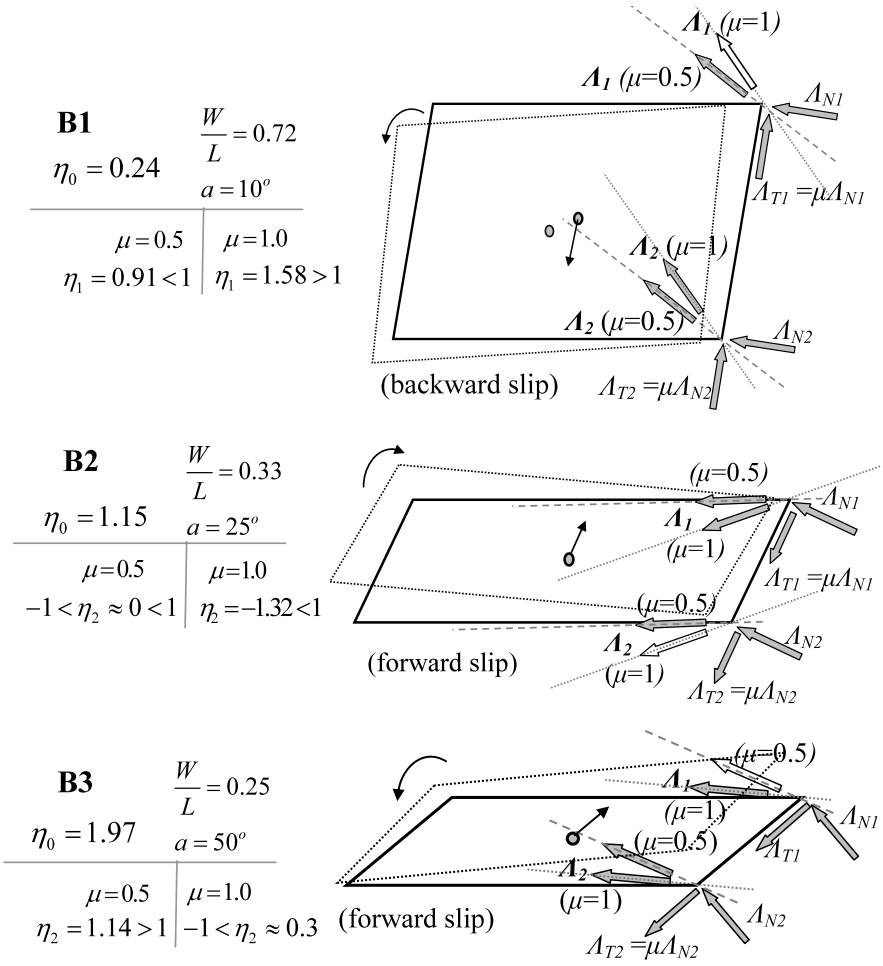

Fig. 11 The double impact of three bridge decks (B1, B2, B3) with increasing dimensionless skew ratios η_0 for two coefficients of friction. *Top*: backward slip, *middle* and *bottom*: forward slip. *Dashed lines* indicate a feasible post-impact position

Fig. 11). The proposed criteria $\eta_{1,2}$ (58) distinguish the double-impact response of a skew body into two distinct types: for $\eta_1 \leq 1$ (backward slip) or $|\eta_2| \leq 1$ (forward slip), double frictional impact results in zero angular velocity and hence zero rotation of the body, otherwise double impact produces angular velocity and hence rotation. Subsequently, the critical curves ($\eta_1 = 1$, $\eta_2 = \pm 1$) of Fig. 10 (and Fig. 12 later on) divide the plane $(W/L, \alpha)$ of skew bodies, depending on the assumed coefficient of friction (μ), into two areas: the one above the pertinent curves wherein $\eta_1 < 1$ (or $-1 < \eta_2 < 1$) holds and the area below the pertinent curves wherein $\eta_1 > 1$ (or $\eta_2 > 1$, $\eta_2 < -1$) holds. Note that double stick is feasible in the gray areas of Fig. 10 provided the transversal–normal velocity ratio γ_T^-/γ_N^- is low enough: $|\gamma_T^-/\gamma_N^-| \leq (1+\varepsilon_N)\mu$.

Figure 10 illustrates that for $\mu = 0$ bridges with modest and high dimensionless skew ratios η_0 (e.g. points B2 and B3 accordingly) rotate after backward slip. On the contrary bridges with small dimensionless skew ratios η_0 (e.g. point B1) do not rotate after backward slip. As μ increases (Fig. 10 bottom, $\mu = 1.0$) so does the tendency of skew bridges to rotate since all three points (B1, B2 and B3) are below the curve $n_1 = 1$ which means that bridges of a wide range of dimensionless skew ratios η_0 rotate, after double backward slip, in such a way that the skew angle increases in accordance with the relevant literature [5]. Figure 10 also shows that after double forward slip only bridges with high η_0 (e.g. B3) rotate, provided the coefficient of friction μ is not high, resulting in increasing the skew angle ($n_2 > 1$). A counter-intuitive rotation which results in decreasing the skew

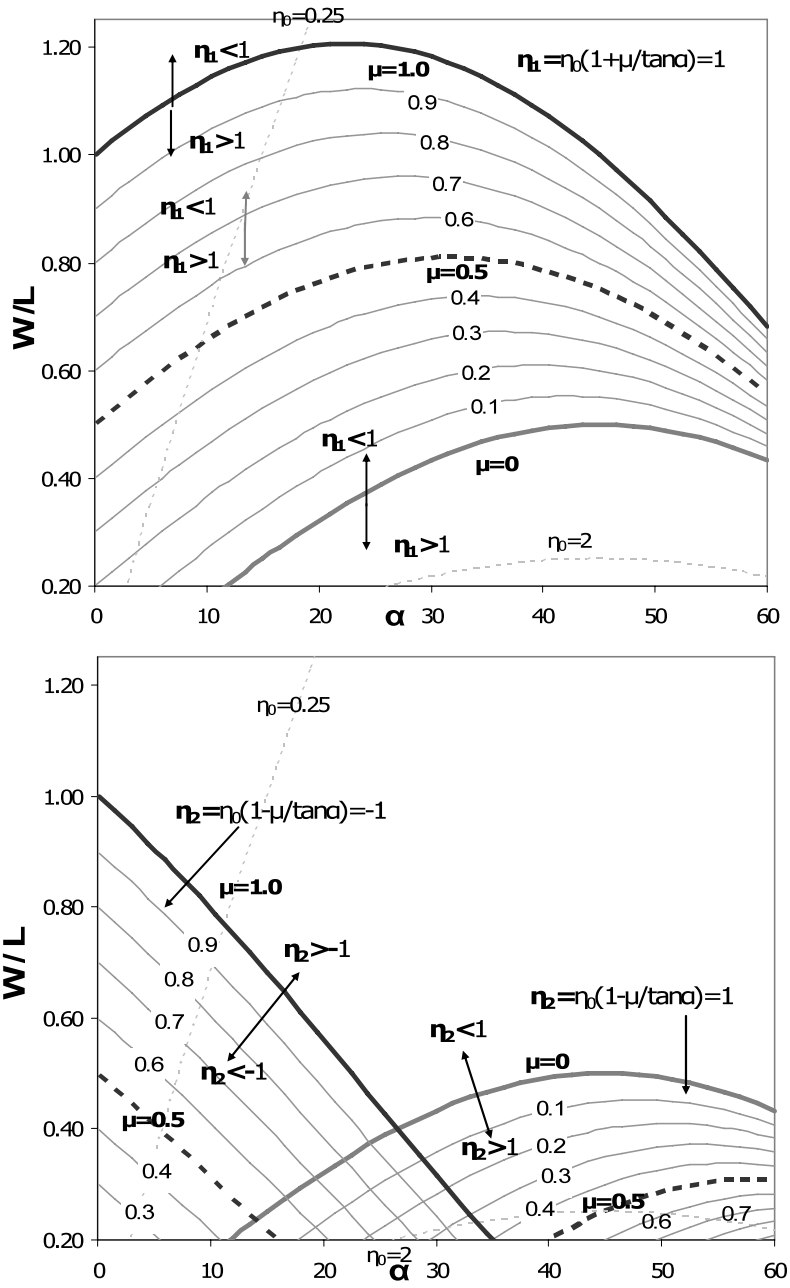

Fig. 12 Critical curves of the proposed criteria $\eta_{1,2}$, in the plane width/length (W/L)–skew angle (α), for different coefficients of friction μ. *Top*: double backward slip, *bottom*: double forward slip

angle, appears after forward slip for small and modest dimensionless skew ratios η_0 (e.g. points B1 and B2) when the coefficients of friction is high ($n_2 > -1$, see also Fig. 11 middle).

Figure 11 illustrates the geometry of the rotational mechanism associated with double frictional impact, which is similar to the frictionless case. When the angular momentums of the resultant impulses are in different directions with respect to the center of mass (C.M.) the angular momentums cancel out and no rotation is developed. On the contrary, when the angular momentums are in the same direction angular velocity and hence rotation is developed. The white arrows in Fig. 11 present impacts that must be ignored since they

violate the inequality constraint $\Lambda_N \geq 0$. As Fig. 11 unveils, the areas wherein $\eta_1 > 1$ and $\eta_2 > 1$ hold, correspond to rotation, after double backward and forward slip (impact) accordingly, in the direction of increasing the skew angle. This trend is in agreement with the relevant literature [5]. On the contrary, the area wherein $\eta_2 < -1$ holds corresponds to rotation, after double forward slip, in the (opposite) direction of decreasing the skew angle. This counter-intuitive rotation is not mentioned in earthquake engineering literature.

Figure 12 presents the critical curves of the proposed criteria for backward slip ($\eta_1 = 1$, Fig. 12, top), forward slip ($\eta_2 = \pm 1$, Fig. 12, bottom) and different coefficients of friction μ. The frictionless case analyzed in the previous section is captured with the $\mu = 0$ curve ($\eta_0 = 1$). Figure 12 shows that most skew bodies tend to rotate after backward slip and not after forward slip since the area wherein $\eta_1 > 1$ holds is broader than that of $\eta_2 > 1$ or $\eta_2 < -1$. As μ increases, the tendency towards rotation in the direction of increasing the skew angle accentuates after backward slip ($\eta_1 > 1$) but diminishes after forward slip ($\eta_2 > 1$). On the other hand, as μ increases the counter-intuitive rotation, in the direction of decreasing the skew angle ($\eta_2 < -1$), becomes feasible after forward slip. This counter-intuitive behavior is more pronounced for small dimensionless skew ratios η_0. It is noted though, that for a specific skew bridge (a specific point in the W/L–α plane) and a given coefficient of restitution, only one of the directions of rotation is feasible to occur after forward slip. In other words the two trends do not coexist.

5.3 Single-frictional impact

Single impacts occur when contact takes place at one corner of the rigid body (Fig. 5, left), i.e. when $\theta^- \neq 0$ and/or $u_\theta^- \neq 0$. Within the context of this paper however, single-frictional impacts can be considered as a special case of the double impact analyzed in the previous section. Each double impact for which $\Lambda_N = 0$ holds at one of the impact points, is in essence a single impact at the other closed impact point ($\Lambda_N > 0$). Hence, using the appropriate lever arms either of the acute ($\tilde{r}_{N1}, \tilde{r}_{T1}$) or of the obtuse corner ($\tilde{r}_{N2}, \tilde{r}_{T2}$) all physically feasible single impacts can be described also with the LCP (11). For example, backward slip at the obtuse corner is described by (51) and existential conditions (52), where instead of r_2 and r_T, $\tilde{r}_{N2}$ and $\tilde{r}_{T2}$ are used. This can be shown also with the comparison of (51), (52), (53), (54), (55), (56), and (57) with the pertinent relations of Payr and Glocker [16] derived from a similar LCP which treats single-frictional impacts.

Figures 13, 14 and 15 illustrate the existential conditions of the three different single-frictional-impact states (forward slip $\Lambda_T = -\mu\Lambda_N$, backward slip $\Lambda_T = +\mu\Lambda_N$ and stick $|\Lambda_T| < \mu\Lambda_N$) in the plane: pre-impact transversal and normal velocity ratio (γ_T^-/γ_N^-)—pre-impact rotation (θ^-). Figure 13 concerns straight bridges i.e. with zero skew angle $\alpha = 0$. Due to the symmetry of the system the response is also symmetrical with respect to rotation. As expected, for frictionless collisions no stick (gray area of Figs. 13, 14 and 15) is observed, whereas as coefficient of friction μ increases the stick area becomes broader. Not so intuitive though, is that the same trend appears as the coefficient of restitution increases.

Figures 14 and 15 present the existential conditions of the three distinct (single-) impact states, for different skew angles α. For positive pre-impact rotations $\theta^- > 0$ impact occurs at the obtuse corner, while for negative rotations $\theta^- < 0$ impact occurs at the acute corner. In bridges the range of rotation values with practical significance is of the order of a few degrees. Within that range, the stick area is systematically broader for (small) positive rotations than it is for (small) negative rotations. This observation is in agreement with the qualitative remarks, found in the literature, that skew bridges tend to jam at the obtuse corner [5]. As the skew angle (α) increases the system becomes less symmetrical and similarly less symmetrical becomes its response with respect to (pre-impact) rotations θ^-. It is also interesting to note that the tendency to stick becomes more pronounced as the skew angle α becomes smaller.

In Fig. 14 (bottom right) for skew angle $a = 30°$, coefficient of friction $\mu = 1.0$ and pre-impact rotations $\theta < -20°$ only two impact states are feasible, backward slip and stick (at the acute corner). In other words, the third impact state, in this case forward slip, is not feasible. This phenomenon is due to the Painlevé paradox [14] which emerges when a critical maximal coefficient of friction is exceeded. However, a detailed discussion on the Painlevé paradox is beyond the scope of this paper which is oriented towards results

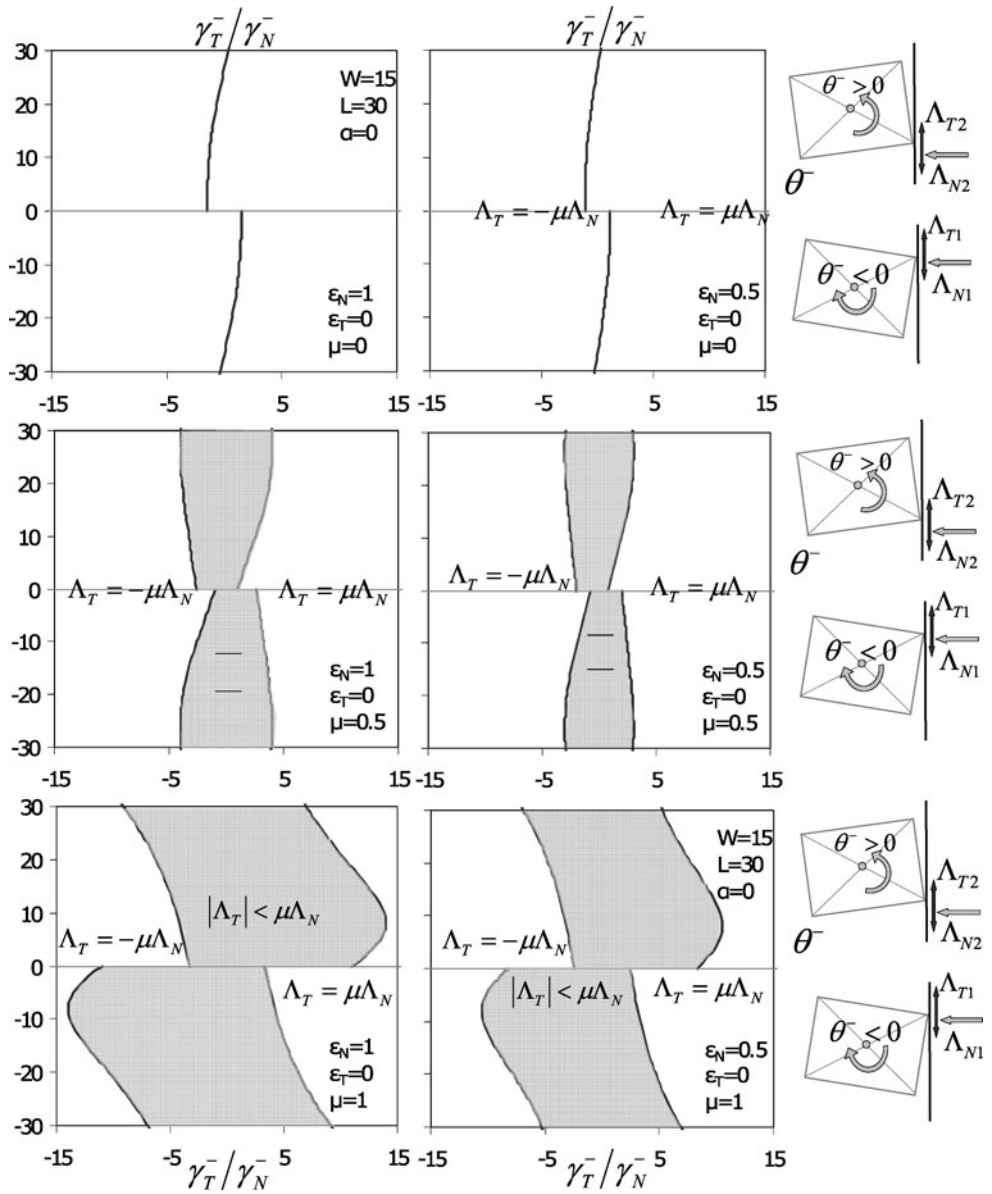

Fig. 13 The three distinct single-frictional impact states in the $(\gamma_T^-/\gamma_N^- - \theta^-)$ plane for straight bridges (zero skew angle $\alpha = 0$). Coefficient of restitution $\varepsilon_N = 1.0$ (*left*), 0.5 (*right*), coefficient of friction $\mu = 0$ (*top*), 0.5 (*middle*) and 1.0 (*bottom*)

applicable to bridges, where (pre-impact) rotations remain within the range of a few degrees.

6 Conclusions

The aim of the present paper is to bring forward the physical mechanism behind deck-abutment collisions in skew bridges. The relevant literature lacks a thorough theoretical study and is mostly confined to empirical descriptions of the phenomenon. Building on the work of other researchers, the study adopts a fully non-smooth rigid body approach and examines in depth the impact response of a planar skew (rigid) body against an inelastic half-space, which encapsulates a lot of the 'physics' involved in deck-abutment collisions.

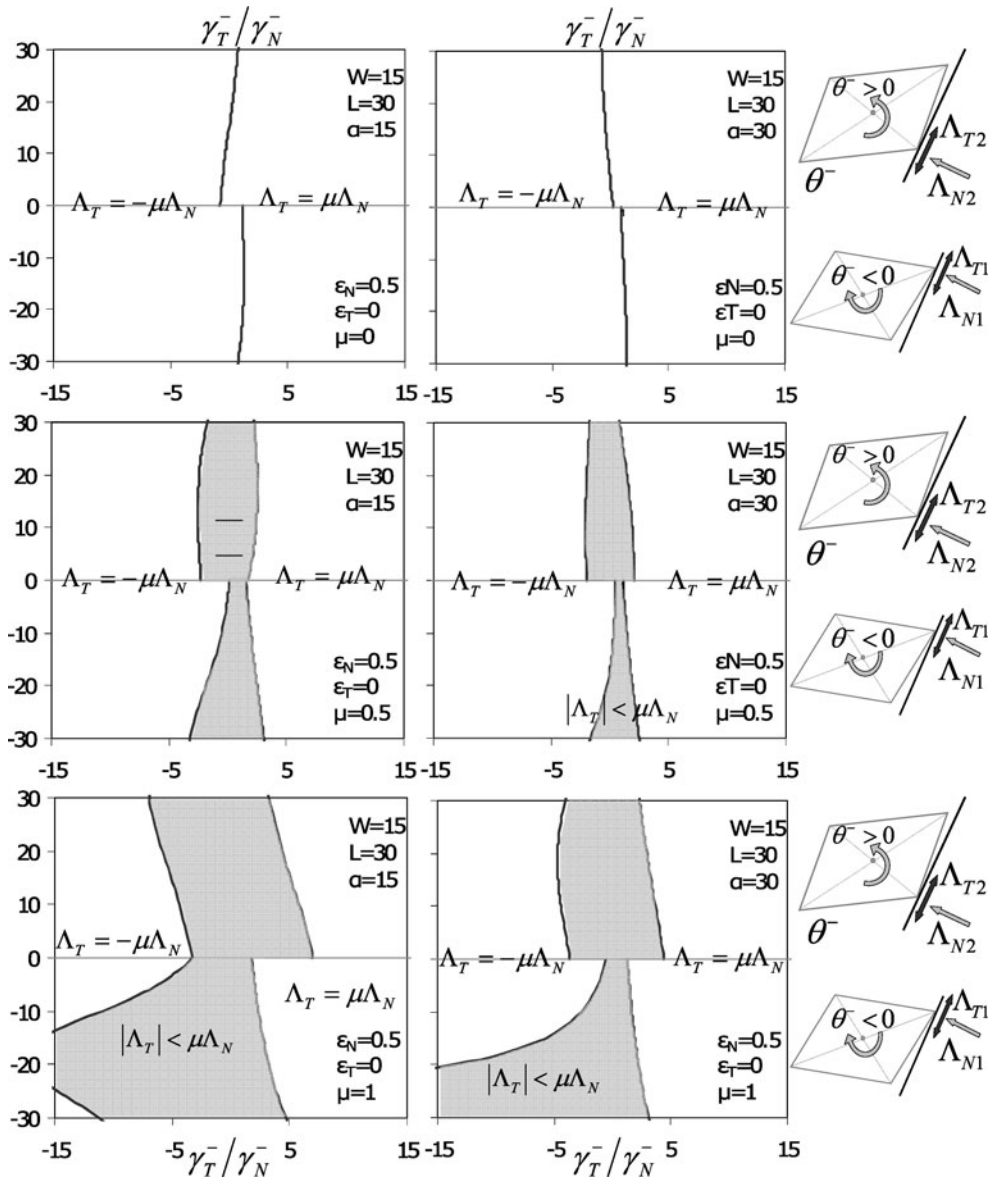

Fig. 14 The three distinct single-frictional impact states in the $(\gamma_T^-/\gamma_N^- - \theta^-)$ plane for coefficient of restitution $\varepsilon_N = 0.5$. Skew angle $\alpha = 15°$ (*left*), 30° (*right*), coefficient of friction $\mu = 0$ (*top*), 0.5 (*middle*) and 1.0 (*bottom*)

The study unveils the rotational mechanism associated with (double) oblique impact and shows that the tendency of skew bridges to rotate depends on the total geometry of the body in plan, not on the skew angle alone, in contrast to what is commonly considered in empirical vulnerability methodologies for bridges. Double oblique impact, either frictionless or frictional, triggers rotation when the resultant impulses of the two impact points produce angular momentums in the same direction with respect to the center of mass. The study also concludes that skew bridges prefer to rotate in such a way that the skew angle increases, in agreement with the relevant literature. However, a counter-intuitive rotation in the opposite direction of decreasing the skew angle, which is caused by friction, is also unveiled.

Frictional oblique impact is treated via a linear complementarity formulation, which includes single

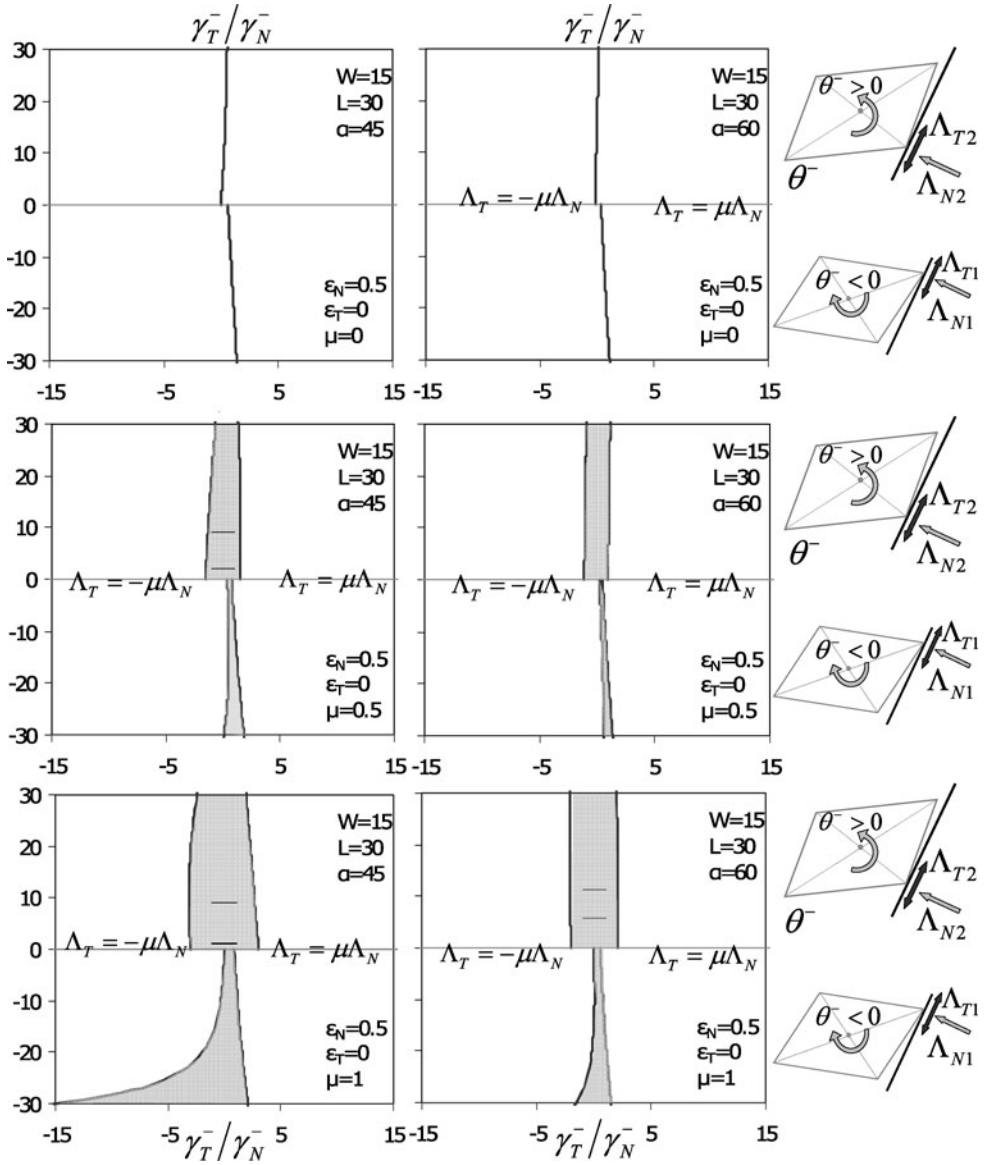

Fig. 15 The three distinct single-frictional impact states in the $\gamma_T^-/\gamma_N^-, \theta^-$ plane for coefficient of restitution $\varepsilon_N = 0.5$. Skew angle $\alpha = 45°$ (*left*), 60° (*right*), coefficient of friction $\mu = 0$ (*top*), 0.5 (*middle*) and 1.0 (*bottom*)

impacts as a special case of the examined double oblique impact. The physically feasible impact states are determined, the pertinent existential conditions are derived and specific criteria are proposed that determine whether double impact triggers rotation. The present analysis finally examines the effect of the impact parameters (coefficient of restitution in the normal direction and coefficient of friction in the transversal direction) on the response and illustrates the complexity of the examined oblique impact.

Acknowledgements The present paper is largely based on the doctoral thesis presented by the author to the Civil Engineering Department of the Aristotle University of Thessaloniki. The writer gratefully acknowledges the valuable contribution of the supervisors Prof. Andreas Kappos and Prof. Nicos Makris in shaping the ideas presented herein.

References

1. Dimitrakopoulos, E.G., Kappos, A.J., Makris, N.: Dimensional analysis of yielding and pounding structures for records without distinct pulses. Soil Dyn. Earthq. Eng. **29**(7), 1170–1180 (2009)
2. Dimitrakopoulos, E.G., Makris, N., Kappos, A.J.: Dimensional analysis of the earthquake response of a pounding oscillator. ASCE J. Eng. Mech. (2009, in press)
3. Dimitrakopoulos, E.G., Makris, N., Kappos, A.J.: Dimensional analysis of the earthquake induced pounding between adjacent structures. Earthquake Eng. Struct. Dyn. **38**(7), 867–886 (2009)
4. EERL (Earthquake Engineering Research Laboratory): Engineering features of the San Fernando earthquake of February 9, 1971. In: Jennings, P.C. (ed.) EERL 71-02 California Institute of Technology, Pasadena (1971)
5. Priestley, M.J.N., Seible, F., Calvi, G.M.: Seismic Design and Retrofit of Bridges. Wiley, New York (1996)
6. EERI: The Tehuacan, Mexico, Earhtquake of June 15, 1999. Special Earthquake Rep. September 1999 EERI, Oakland (1999)
7. Kim, S.H.: GIS-based regional risk analysis approach for bridges against earthquakes. Dissertation, Department of Civil Engineering, State University of New York at Buffalo (1993)
8. Maragakis, E., Jennings, P.C.: Analytical models for the rigid body motions of skew bridges. Earthquake Eng. Struct. Dyn. **15**, 923–944 (1987)
9. Maleki, S.: Seismic modeling of skewed bridges with elastomeric bearings and side retainers. ASCE J. Bridge Eng. **10**(4), 442–449 (2005)
10. Moreau, J.J.: Unilateral contact and dry friction in finite freedom dynamics. In: Moreau, J.J., Panagiotopoulos, P.D. (eds.) Non-Smooth Mechanics and Applications, CISM Courses and Lectures, vol. 302, pp. 1–82 Springer, New York (1988)
11. Panagiotopoulos, P.D.: Dynamic and incremental variational inequality principles, differential inclusions and their applications to co-existent phases problems. Acta Mech. **40**, 85–107 (1981)
12. Panagiotopoulos, P.D.: Noncovex energy functions. Hemivariational inequalities and substationary principles. Acta Mech. **48**, 111–130 (1983)
13. Glocker, C.: Set-Valued Force Laws. Springer, Berlin (2001)
14. Brogliato, B.: Nonsmooth Mechanics, 2nd edn. Springer, London (1999)
15. Leine, R.I., van Campen, D.H., Glocker, C.: Nonlinear dynamics and modeling of various wooden toys with impact and friction. J. Vib. Control **9**, 25–78 (2003)
16. Payr, M., Glocker, C.: Oblique frictional impact of a bar: analysis and comparison of different impact laws. Nonlinear Dyn. **41**, 361–383 (2005)
17. Brogliato, B., ten Dam, A.A., Paoli, L., Ge'not, F., Abadie, M.: Numerical simulation of finite dimensional multibody nonsmooth mechanical systems. Appl. Mech. Rev. **55**(2), 107–150 (2002)
18. Pfeiffer, F.: Nonsmooth dynamics in engineering. In: Nonsmooth/Nonconvex Mechanics with Applications in Engineering, II. NNMAE—Proceedings of the International Conference. In MEMORIAM of Professor P.D. Panagiotopoulos, 7–8 July 2006, Thessaloniki, Greece, pp. 295–306 (2006)
19. Kwack, B.M., Lee, S.S.: A complementarity problem formulation for two-dimensional frictional contact problems. Comput. Struct. **28**, 469–480 (1988)
20. Klarbring, A., Bjrrkman, G.: A mathematical programming approach to contact problem with friction and varying contact surface. Comput. Struct. **30**, 1185–1198 (1988)
21. Pfeiffer, F., Glocker, C.: Multibody Dynamics with Unilateral Contacts. Wiley, New York (1996)